2013

Embedded Nanosensors for defect identification using flexible, optically transparent, deformation responsive wrinkled Single Walled Carbon Nanotube meshes

Pallavi Anipindi
West Virginia University

Embedded Nanosensors for defect identification using flexible, optically transparent, deformation responsive wrinkled Single Walled Carbon Nanotube meshes.

By

Pallavi Anipindi

Master's Thesis submitted to the

College of Engineering and Mineral Resources

In partial fulfillment of the requirements for the degree of

Master of Science

In

Mechanical Engineering

APPROVED, THESIS COMMITTEE:

Dr. Daneesh Simien, Professor
Committee Chair,
Mechanical and Aerospace Engineering

Dr. Xueyan Song, Assistant Professor
Mechanical and Aerospace Engineering

Dr. Clayton Simien, Research Asst. Professor
Department of Physics, Eberly College of Arts and Sciences

Department of Mechanical and Aerospace Engineering

West Virginia University, Morgantown

June 2013

Keywords: Wrinkled Carbon nanotubes, homogeneous length separation, Crack detection, SWCNTs as sensors

ABSTRACT

Embedded Nanosensors for defect identification using flexible, optically transparent, deformation responsive wrinkled Single Walled Carbon Nanotube meshes.

Pallavi Anipindi

Most structures such as buildings, pipelines carrying natural gas, nuclear plant cooling tanks and so forth are made of concrete. In vivo detection of the onset of cracks and voids in these concrete structures have many barriers and neglecting those could lead to failure of structures causing loss of properties and damage to lives. Embedded single walled carbon nanotubes (SWCNTs) with exceptional mechanical, optical, and electrical properties can be utilized in overcoming these barriers. This type of NDT technique can monitor the potential for failure in concrete structures by allowing us to monitor the cracks from the atomistic level. It has been shown that the use of randomly distributed homogenous length sorted SWCNTs offer large active areas with high current output. Here we attempt to wrinkle SWCNTs configurations with high mechanical flexibility and stretchability which may in the future prove to be a diagnostic tool in various matrices as cracks are initiated. We investigated the use of these wrinkled SWCNT meshes in concrete material and monitored their conductivity response at the moment of crack initiation, voids and inclusion defects. SWCNT meshes are not only useful in recognition of cracks but also can be formed as useful nano-composites.

Key words: Carbon nanotubes, wrinkling, homogeneous length separation, Crack detection, SWCNTs as sensors.

ACKNOWLEDGEMENT

My graduation life in West Virginia University has been educating and wonderful journey. I loved every moment of my grad life, which included challenging coursework, research and joyful instances with friends. It is now time to acknowledge all of the individuals and sources that have been a crucial influence throughout my graduate career.

I take this opportunity to sincerely thank my professor Dr. Daneesh Simien, for providing me such an interesting and challenging topic. Your advice when ever needed helped me to improve my thought process. Thanks a lot for imparting your knowledge. I thank my committee members Dr. Clayton Simien for teaching me laws of physics and helping me in every aspect of my research. I thank Dr. Xueyan Song for giving me necessary inputs when ever needed and being a part of my committee. I also thank Dr Mourad Riad for his constant support on concrete testing, valuable inputs in the field of Science and Engineering which helped me in successful completion of my project.

I thank my parents Ramesh Kumar Anipindi, Lalitha Devi Anipindi, Appa Rao Anipindi, Lakshmi Anipindi, my fiancé Balakrishna Ayyagari, my sisters Soujanya Nookala, Neerajakshi Viswanatha, brother's-in Law Bhaskar Nookala, Vijay kumar Viswanatha, other relatives and friends for their guidance and moral support.

I would like to thank my colleagues Sai Praneeth Gunturu for motivating me and supporting me throughout the project, Prudvi Raavi Teja and Suvineeth Ramayanam, who were very helpful in the lab. I really enjoyed miscellaneous discussions we had. I am thankful to Lekha Kuchipudi for being such a fantastic friend and guide. I also thank Manohar Gaddipati, Saurabh Chaudhari, Arkamitra Kar, Savan Suri, Anveeksh Koneru for inspiration and motivation.

Finally, I would like to thank, WVU shared research facility faculty members Dr. Marcela Redigolo**,** Dr. Kolin S. Brown, Dr. Weiqiang Ding, Dr. Siera Talbott, Harley Hart and WVU faculty and staff for their essential inputs. WVU will always be a sweet and memorable chapter in my life.

TABLE OF CONTENTS

LIST OF FIGURES

LIST OF TABLES

NOMENCLATURE

ASTM : American Society of testing and Management

CNTs : Carbon Nanotubes

CoMoCAT : Cobalt Molybdenum Catalyst

CVD : Chemical Vapor Depsition

DC : Direct Current

DGU : Density Gradient Ultracentrifugation

DI : De-ionized

DOC : Sodium Deoxy Cholate

ECC : Engineered Cementitious Composites

EIS : Electrical impedance spectroscopy

EIT : Electrical Impedance Tomography

HPLC : High Performance Liquid Chromotography

MPa : Mega Pascals

NDE : Nondestructive Evaluation

NDMT : Non-destructive material testing

PDMS : Poly dimethy siloxane

PS : Polystyrene

RBM : Radial Breathing Mode

SEM : Scanning Electron Microscope

SWCNTs : Single Walled Carbon Nano Tubes

UTM : Universal Testing Machine

UV-Vis-NIR : Ultra Violet Visible Near Infrared

Chapter 1

INTRODUCTION

Most structures such as buildings, bridges, dams, roads which are considered as basic infrastructure of a society are built using concrete as a base material. Concrete which is mixture of gravel, crushed stone and cement with water forms a composite material. These composites materials are used as filler and binder. Binder, mixture of cement, sand and water acts as a "glue". Binder and filler together form a synthetic conglomerate [1]. Although, there are many reasons external loads, corrosion, thermal stress and many more for failure of the structures, this thesis focuses solely on binders which are a mixture of cement, sand and water.

Strength and durability of the binders are important features to be considered and monitored. Damage in the binders can occur due to environmental deterioration, detailing, chemical reaction aging, thermal stress, corrosion, increased load, poor construction practices, construction overloads, and errors in design [2, 3].

Electromagnetic radiation, ultrasonic, magnetic particles liquid penetration, radiographic, low coherence interferometry and eddy current testing are some of the techniques that are in existence to evaluate the state of material or component. However the drawbacks of such techniques are that they are used as external instrument to evaluate the material/component state.

The motivation of this project is to develop a nondestructive diagnostic tool with the use of embedded wrinkled SWCNTs which could be incorporated into various matrices very easily. It has been shown that the use of randomly distributed homogenous length sorted SWCNTs offer large active areas with high current output with orientation of individual tubes as a whole [4]. This project aimed to develop a diagnostic tool using wrinkled SWCNTs as they provide more flexibility and stretchability without compromising optical properties [5-7].

1.1 General Composites

General composites are formed by combination of two or more distinctive and separate materials to form single new material with properties that are different form either of the constituent material.

Depending on the functionality of the material, constituent materials are classified into two categories:

a) Fibers

b) Matrix

Dominant function of fibers is to carry load and provide stiffness to the material. Carbon/graphite can be considered as best example for fibers. Matrix are generally weaker and were flexible than fibers.

Mixture of Cement, sand and water are considered as matrix in this case as they are weak when compared to SWCNTs. SWCNTs are one among the strongest material ever known to man. SWCNT are continuous chain of carbon atoms with bonder order of 1½. Higher the bond order, lower is the length of the bond, this is one of the reasons for nanotubes to be stable [8-10]. Hence, SWCTs acts as fibers that provides strength to matrix.

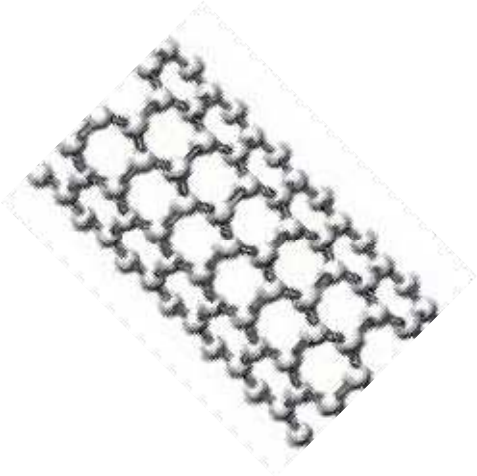

Figure 1: Schematic Diagram of SWCNTs, shows continuous chain of carbon atoms

Chapter 2 discusses about the progress in science in using carbon nanotubes carried by various research groups and scientists. Some of the research groups illustrated the advantage of using mixed length CNTs and homogeneous length sorted CNT. But our project aims to develop a sensor with homogeneous length sorted and wrinkled CNT meshes that can efficiently detect micro-cracks in concrete structures.

Chapter 3 details about Carbon nanotubes structure and their applications. We discuss the length sorting process and various characterization techniques carried out in this work. Characterization

of SWCNTs was carried out using UV-Vis NIR spectroscopy, Raman spectroscopy, SEM and optical microscopy to study the optical properties, degree of length separation, wrinkling parameters. Chapter 4 gives the material properties of the concrete materials and also other chemicals and solvents. Chapter 5 deal the sensor fabrication, testing the samples made for studying the sensors during crack development. The identification of micro-cracks in concrete specimens was studied by measuring impedance across the sample as a function of strain. Three length groups of CNTs were wrinkled with two varied strain percentages and were used a sensors in this study. Chapter 6 discusses the results obtained from the samples which in turn demonstrates a relationship between crack propagation and impedance which identifying cracking. Chapter 7 presents the conclusions and future work.

Chapter 2

BACKGROUND

2.1 Introduction

Carbon nanotubes are rolled graphene sheets forming a fullerene structure or honey comb structure from the sp^2 arranged carbon atoms. They can be classified a single walled carbon nanotubes or multi-walled carbon nanotubes [32]. Extensive research in the field of carbon nanotubes proved to have wide range of applications in health, environment, electronics, and composites. This motivated researchers to use these carbon nanotubes as composite material for concrete and simultaneously help in detecting the micro-cracks and voids in the concrete structures. This process of identifying defects in concrete structures is termed as "Structural Health Monitoring" and smart materials like the carbon nanotubes were incorporated into structures to identify the defects [4].

2.1.1 Crack detection in concrete structures using EIT methods

Crack propagation in concrete structures is resulted from externally applied loads, stresses and shrinkage. The cracks generally obtained belong to two categories, one which affects the external aesthetics of structure and other which reduces strength, stiffness and durability. Initially detailed visual inspection helps out in identifying cracks and later any suspicious cracks encountered can be studied through non-destructive testing techniques like ultra sonic inspection. Electrical impedance tomography (EIT) technique is used for measuring internal strain fields across 2D or 3D engineered cementitious composites (ECC). Since cracks are non-conducting across their widths, EIT helps in imaging cracks as conductivity reductions occur.

EIT is a more advanced approach to measure material conductivity as the two- and four-point probe methods suffer from restrictions while used to characterize electrical properties in cement like materials. From this, we can conclude that EIT is a powerful NDE tool which offers multi-dimensional sensing that can help in locating cracks in cementitious structures. However, EIT is helpful in detecting cracks in ECC but cementitious materials such as concrete must be explored yet [11].

2.1.2 Application of carbon nanotubes for non-destructive material testing

Many structures and components need frequent monitoring and this could be done with visual inspection and other non-destructive testing techniques. For structures which have limited access like the nuclear plant cooling tanks and gas pipelines etc, incorporation of the smart materials into their structures help in structural health monitoring. This new approach of using smart materials for NDMT improves the reliability and reduces maintenance and inspection based costs [12].

2.1.3 Embedded Carbon nanotube sensors for damage detection in concrete structures

The deterioration of concrete structures due to various factors like ageing, unanticipated stresses, environmental impacts have accentuated the need for structural health monitoring to keep a track of the safety of structures and improve their performance. So, the structural health monitoring requires the integrity of carbon nanotubes-smart materials with the civil structures. The exceptional properties of carbon nanotubes help in the detection of cracks at an early stage through change in impedance helps in preventing catastrophic failures [13].

Most researchers have incorporated carbon nanotubes for structural health monitoring by dispersing them into various matrices like concrete and polymers but poor dispersion, alignment and adhesion of the CNTs were observed [12].

The architecture of SWCNT meshes were controlled and monitored to have mechanical flexibility and stretchability without compromising optical transparency [14].

2.1.4 Motivation behind using wrinkled carbon nanotubes

The wrinkled carbon nanotubes replace the large scale NDT equipment which was used for failure analysis. These wrinkled SWCNT meshes give electrical signals to computers with the initiation of crack of nanometers order [14].

The orientation and interaction dynamics in length sorted single-walled carbon nanotubes can be controlled and monitored by percolation and wrinkling. This is very important for developing robust flexible meshes for electronic applications. Strained elastomeric substrates are generally used to produce sinusoidal wave like structures.

Wrinkled thin films of CNTs have large surface coverage which makes them ideal for various applications as they exhibit sharp changes in their optical and conductivity properties [14].

2.1.5 Nano materials to improve strength and permeability of concrete

Recent studies show that nanotechnology has been introduced in the production of concrete to reduce permeability, as it helps extending service life of concrete. As supplementary cementitious materials in concrete densify the cement matrix and their large surface area can fill the voids in the cement matrix this shows improvements in strength, ductility, and impact resistance [15]. Carbon nanotubes added to the cement matrix improves matrix tensile strength and fracture energy as the surface can be bridged with CNTs [40].

The interaction between carbon nanotubes and cement hydrates improves bond strength and cement acts as bridge between cracks and voids. Research has been shown that incorporation of carbon nanotubes in cementitious system can control cracking through bridging and load transfer across cracks and pores [16].

2.2 Conclusion

The research conducted up to present date using CNTs in cementitious structures, indicate that CNTs have very good potential in sensing cracks and type of defects in concrete structures. As the sensitivity of the CNTs improves with the increase in surface of contact, concentration and percolation factors, focus should be made upon the usage of SWCNT wrinkling architectures as sensors in concrete materials and their effect as composites can also be studied. These wrinkled SWCNTs embedded in concrete structures can be subjected to tension under three point bend test and the change in impedance across the sample can be studied which indicates the propagation of micro-cracks.

Chapter 3

SINGLE WALLED CARBON NANOTUBES AND ITS CHARACTERIZATION

3.1 Carbon Nanotubes

Rolling up a graphene sheet produces carbon nanotubes which are identified as one among the best nano materials which has unique mechanical, electrical and thermal properties [17]. CNTs have high aspect ratio (length to diameter ratio) and their tensile strength is nearly hundred times that of steel at one sixth of the weight. CNTs have high current carrying capacity than copper and gold. Semiconducting species have higher electron mobility than silicon; thermal conductivity is close to in-plane graphite. CNTs have distinct optical absorption and fluorescence response making them highly transparent which gives competition to ITO as transparent conductor [18]. This research on carbon nanotubes led to advancements in nanotechnology field for various applications including transistors and sensors.

3.2 Synthesis of CNTs

CNTs were earlier synthesized by high temperature methods (above 1700ºC) like arc discharge method or laser ablation. The orientation, alignment, length, diameter, purity and density of CNTs can be managed by a low temperature technique (less than 800ºC) called the chemical vapour deposition (CVD) [19].

3.2.1 Arc Discharge

CNTs with less structural defects are produced in this method when compared to other techniques and higher temperatures (above 1700ºC) are used in this method [19]. This process involves immersing of two graphite rods in an inert gas like He and a direct-current arc is applied across them to produce CNTs. Single walled CNTs are generated when graphite anode contains a metal catalyst (Fe, CO) with a pure graphite cathode [20].

3.2.2 Laser Ablation

SWNTs were produced when the laser hits the carbon targets containing graphite and cobalt/nickel composite that is placed in a 1200°C quartz tube furnace under the argon atmosphere. The nanotubes will form from carbon vapors and condense on the walls of the flow tube [21].

3.2.3 Chemical Vapor Deposition

Chemical vapor deposition (CVD) has become a common technique to grow CNTs in the last decade, with the interest of capable to be scaled for industrial production. Regardless of the applications and growth approach, the ability to control the properties of the nanotubes is critical to realize the promise of carbon nanotubes [22].

3.3 Classification and structure of CNTs

3.3.1 Classification and applications of CNTs

The application of CNTs usually varies by the classification of their structure depending on the specific properties given by diameter, length, number of walls, chiral angle, etc. The recent applications of CNTs discovered include conductive films, solar cells, fuel cells, super capacitors, transistors, memories, displays, separation membranes and filters, purification systems, sensors, clothes, sports equipment, etc [20].

3.3.2 Structure of CNTs

CNTs are obtained by rolling a graphene sheet in a specific direction and keeping the circumference of the cross-section constant (a seamless cylinder). The number of sheets rolled determines the walls of the tubes like single walled, double walled and multi-walled CNTs. The orientation gives the types of CNTs like the metallic and semi-conducting tubes [23]. These SWCNTs are an allotrope of sp^2 hybridized carbon with cylindrical structure having one or both ends capped with hemispherical Bucky ball or fullerene structures.

Figure 2, describes the Chirality and indices of a graphene sheet defined with chiral vector $\mathbf{C}_h$ and angle θ. The chiral vector is formulated by equation (1) in terms of the lattice translational indices (n, m) integers representing the steps of carbon bonds of the lattice and the unit vectors $\mathbf{a}_1$ and $\mathbf{a}_2$.

$$C_h = na_1 + ma_2 \quad (1)$$

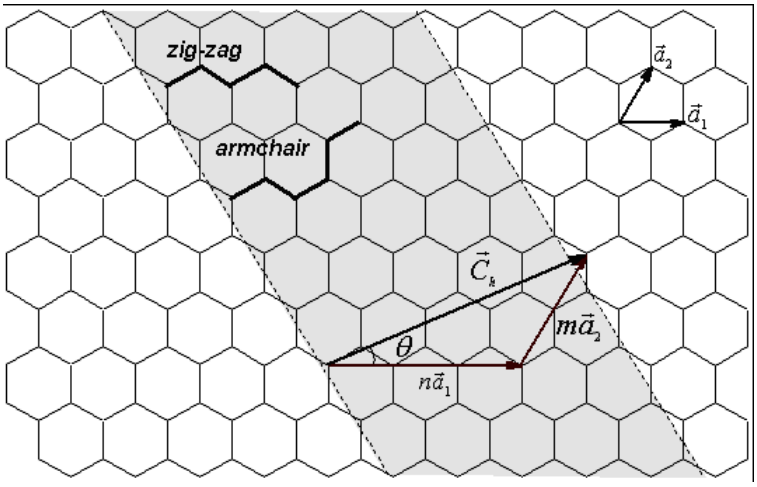

Figure 2: Schematic Diagram of SWCNTs, shows atomic structure of CNTs [17]

The degree of "twisting" of the tube, is defined by the angle (θ) (chiral angle) between the vectors $\mathbf{C}_h$ and $\mathbf{a}_1$, which varies in the range of $0^o \leq |\theta| \leq 30^o$. In terms of the integers (n, m), θ can be described by the set of equations below [2]:

$$\sin\theta = \frac{\sqrt{3}m}{2\sqrt{n^2+m^2+nm}}$$

$$\cos\theta = \frac{2n+m}{2\sqrt{n^2+m^2+nm}} \qquad (2)$$

In figure 3 (a) represents the structure of armchair ($\theta = 30^o$) and (b) zig-zag ($\theta = 0^o$) and (c) when $0^o < |\theta| < 30^o$, chiral carbon nanotubes. A nanotube is armchair for (n, m) and zigzag for (n, 0) in terms of the chiral vector and this determines the metallic nature of CNTs, armchair represents metallic tubes and zig-zag represents semiconducting tubes [23].

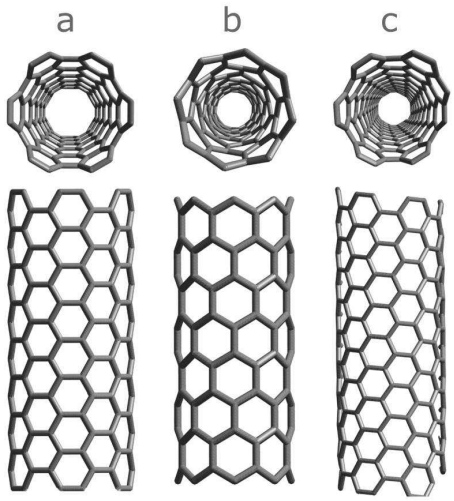

Figure 3: Schematic diagram of (a) an armchair SWCNT, (b) a zig-zag SWCNT, and (c) a chiral SWCNT (reproduced from [2]) [23]

3.4 Homogeneous length separation of Carbon nanotubes

The Cobalt Molybdenum catalyst (CoMoCAT) carbon nanotubes were used for creating length sorted wrinkled SWCNT mesh networks which acted as sensors in identifying cracks in concrete structures. These CNTs are in powdered form in various lengths bundled together with impurities. In this project, we focused on separating the nanotubes length wise in order to incorporate them into concrete matrix and to study the effect of sensing properties of each length of nanotubes along with varied wrinkle rates. In order to achieve defect free length sorted nanotubes, various techniques were followed worldwide. These techniques include Capillary electrophoresis, gel electrophoresis, liquid-liquid extraction, and size extraction chromatography [24]. Yuki Asada et al showed that DNA wrapped SWCNTs were sorted by length using size exclusion high performance liquid chromatography (HPLC). They used purified HiPco SWCNTs and CoMoCAT SWCNTs and sorted them according to length [25]

3.4.1 De-bundling and Purification of SWCNTs

SWCNTs powder purchased from South West Nanotechnologies were in clustered form having different length SWCNTs along with impurities. Two tasks should be accomplished before separating the CNTs by length. First task was to break the CNT clusters by dispersing 1mg of SWCNT powder in 1ml of 2% DOC (Sodium De-oxycholate solution). The resultant soapy

solution was sonicated in a Misonix Micro tip Ultra sonicator for 90 minutes with amplitude set to 60. This mixture was put in an ice bath to reduce the heating effect caused by the sonicator, as the produced heat would damage the SWCNTs. Figure 4 shows the Misonix Micro tip ultra-sonicator.

Figure 4: Shows the Misonix ultra-tip sonicator used for de-bundling the CNTs

A Sorvall WX Ultra series centrifuge with Surespin TM 620/36 rotor was used to obtain pure SWCNTs through centrifugation process. The sonicated SWCNT solution was filled in 37 ml buckets and was centrifuged for 2 hours at 17800 RPM. In this process denser materials settle down and lighter materials travel upwards because of the action of centrifugal force. As the impurities are denser than the SWCNTs, they settle down at the bottom and the supernatant containing de-bundled SWCNTs settle on the top. Supernatant was pipette out and further was used for length separation and the impurities were separated successfully.

3.4.2 Homogenous length separation of SWCNTs using Ultra centrifugation method

Homogenous length separation of SWCNTs was done by Thermo Scientific's Sorvall WX Ultra series centrifuge with Surepin TM 630/36 rotor was used. Figure 5 represents the image of centrifuge used for length separation of CNTs.

Figure 5: Shows the image of the Thermo scientific Sorvall WX Ultra-series Ultra-centrifuge used for length separation of CNTs

Rotor of the centrifuge had 6 buckets each of capacity 37ml which was filled with the following constituents: 2.5ml of 40% W/V Iodixanol and DOC; 2.5 ml of 30%W/V Iodixanol, DOC; 4ml of 20% W/V Iodixanol, SWCNTs and DOC and remaining with 18% W/V Iodixanol, DOC and DI water were filled from bottom to top in each tube respectively. These layers form a linear density gradient which helps in length separation when subjected to centrifugation. These tubes were weighed equally and then the rotor was placed in the centrifuge and rotated with 11500rpm at room temperature for 87 hours and 27 minutes. Figure 6 shows the preparation of density gradient and the length separation of CNTs after centrifugation process.

a) b)

Figure 6: a) Shows the image of preparation of linear density gradient and b) shows the solution after length separation of CNTs

The effect of centrifugation led to the CNTs present in the solution to settle and sort into layers according to length because of buoyancy and fractional forces. The flux N_i of each species i, was modeled according to Nernst-Planck formulation as shown in equation 3 [26].

(3)

Given the average parameters for the separation of particles in equation 4 as,

$$\left|\frac{c_i F_{buoyancy}}{f_i}\right| \gg |D_i \nabla c_i| \tag{4}$$

Where in diffusive flux can be neglected from equation

Buoyant force can be calculated using equation 5,

$$F_{buoyancy} = \pi r^2 l * (\rho_s - \rho_{swcnt}) * G \tag{5}$$

Where,

r – Radius of the SWCNT plus the surfactant shell,

l – Tube length

ρ_s – density of the solution

$\rho_{swcnt,i}$ – density of SWCNT (plus its surfactant shell)

G – Centripetal acceleration

Reynold's number, $Re = V_i \rho_s l/\eta \ll 0.1$

Ballistic velocity of SWCNT,

friction factor for parallel and perpendicular surfaces is given by set of equations 6,

$$V_i(l) = F_{byouyancy}/f_i$$

$$f_{\parallel} = \frac{\pi \eta l}{\gamma}\left(\frac{1 + {0.307}/{\gamma}}{1 - {0.5}/{\gamma}} + {0.426}/{\gamma^2}\right)$$

$$f_{\perp} = \frac{\pi \eta l}{\gamma}\left(\frac{1 + {0.307}/{\gamma}}{1 - {0.5}/{\gamma}} + {0.119}/{\gamma^2}\right) \tag{6}$$

$where \quad \gamma = ln\left({l}/{\gamma}\right)$

γ(gamma) – overlap integral

η(eta) – fluid viscosity

Therefore, the flux in terms of concentration and overlap integral is given by equation 7 [26],

$$N_i(l) \approx c_i \frac{(\rho_s - \rho_{swnt,i}) G r^2}{\eta} \frac{\gamma^4 + 0.614\gamma^3 + 0.3883\gamma^2 - 0.3943\gamma}{2\gamma^3 + 0.044\gamma - 0.1535} \tag{7}$$

$$for\ \Delta\rho = \rho_s - |\rho_{swnt}| \gg \Delta\rho_{swnt} = |\rho_{swnt}| - \rho_{swnt,i}$$

This theory proved that the separation of the nanotubes according to length was done ultra centrifugation as the longer length CNTs travel to the top of the column and leaving the smaller CNTs at the bottom. 16 fractions were collected with 2ml in each vial and later various characterization techniques were implemented to observe the length separated CNTs as shown in Figure 7.

Figure 7: Shows the image of the vials of 16 fractions collected from the centrifuge tube after centrifugation

3.5 Sample preparation procedure for characterization of Single walled carbon nanotubes

The effect of wrinkled and length varied SWCNTs embedded into concrete structures for detecting cracks was studied in this project. Therefore it is very essential for us to verify the lengths, diameter and wrinkling parameters of SWCNTs. The solution that was obtained after centrifugation consists of a mixture of SWCNTs, Sodium Deoxycholate, Iodixanol, and Deionized (DI) water. To characterize SWCNTs, they were separated from the above mentioned mixture. The following is the protocol followed for each respective characterization technique. Hence forth, SWCNTs that were separated into vials were referred to SWCNT solution.

3.5.1 Sample preparation protocol of individual SWCNTs for Raman Characterization

Characterization of SWCNTs on Raman spectroscopy was done using the dialysis technique as mentioned in section 5.4.3.1. The carbon nanotubes solution obtained after centrifugation was used in this process. 200 µl of SWCNT solution mixture was dropped on a 0.05 µm VMWP cellulose membrane purchased from Millpore. 50x amount of isopropane alcohol mixed in DI water in 1:4 ratios was added to the SWCNTs solution and air was supplied to the system to

wash leftover surfactant and chemicals. Thus obtained CNTs on the cellulose membrane were transferred on to a cleaned silicon wafer by pressing the cellulose number against it.

3.5.2 Sample preparation protocol of individual and wrinkled for SWCNTs SEM

To image the SWCNTs using Scanning electron microscope, the salts present in the solution along with SWCNTs were removed using dialysis technique. The fractions obtained after centrifugation of 87 hours and 27 minutes contained Sodium-deoxycholate, Iodixanol along with SWCNTs which contributed for charging up the sample while imaging in SEM. So, proper technique for removal of these salts was implemented using dialysis process as mentioned in 5.4.3.1 section. Sample preparation technique for observing well dispersed SWCNTs in SEM was followed as in section 3.5.1

For observing wrinkled SWCNTs and their parameters, sample was prepared using vacuum filtration as mentioned in section 5.4.3.1. Here PDMS was the substrate pre-strained as per the required strain rates, on which SWCNTs were deposited using vacuum filtration method.

3.6 Characterization of individual and wrinkled SWCNTs

3.6.1 UV Vis NIR Spectroscopy

UV-Vis NIR Spectroscopy gives the absorbance peaks of single walled carbon nanotubes dispersed in a solution which tell about their chirality and types. This data is required for embedding the type of SWCNTs into concrete matrix [33].

A Perkin Elmer high performance Lambda UV-Vis-NIR spectrometer of model 750, specially designed for material science application was used for characterizing SWCNTs. Every SWCNT present in a solution absorbs light energy when the excitation wavelength is equal to the excitation energy of electrons to excite from valence band to conduction band. The spectrum obtained through UV-Vis NIR spectroscopy showed variation in the intensity of absorption when the spectra were normalized at 775nm where there were no π plasmon transitions. The spectra also illustrated the presence of optical characteristics at $E^{s}_{11,}$ $E^{s}_{22,}$ $E^{m}_{11,}$ and E^{s}_{33} electronic transitions of metallic and semi-conducting bands [27, 33].

Figure 8 represents UV-Vis NIR spectra of the 16 fractions obtained from the length sorting process of the SWCNTs. Spectrum of each fraction was taken in the range of 160nm to 1800nm

at an interval of 1nm. To obtain the spectra of pure SWCNTs, subtraction of the spectra of DOC and Iodixanol was done after normalizing the spectra at 775nm. This determines the purity or homogeneity of SWCNTs.

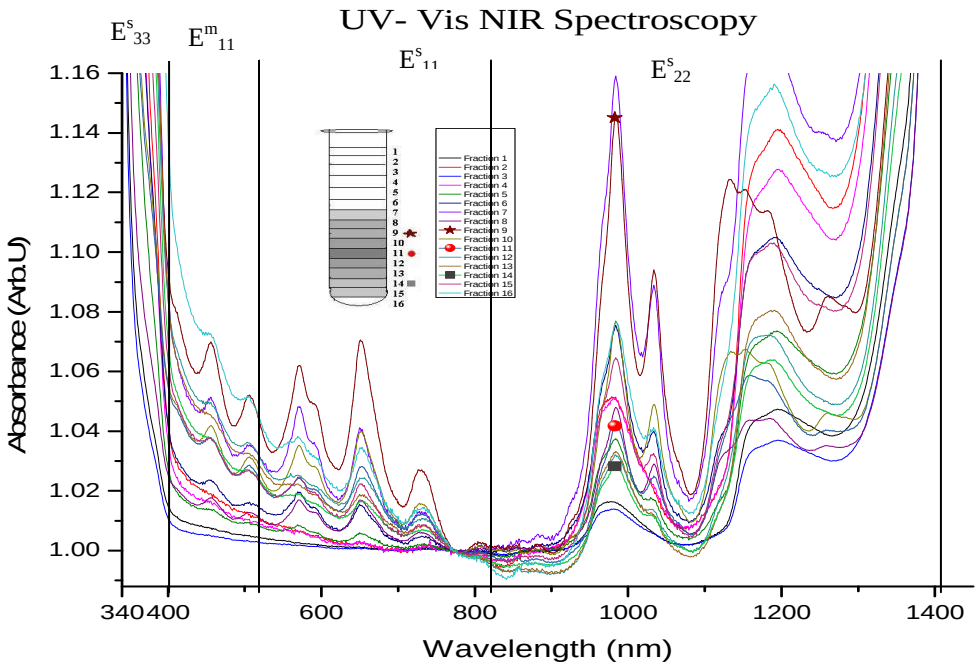

Figure 8: Represents optical absorbance spectra of 16 fractions obtained from length separation process, normalized at 775nm and subtracted from the DOC and Iodixanol spectra

UV-Vis NIR spectra was collected by taking 1ml of solution from each fraction into a quartz cuvette of path length 1mm. When the excitation wavelength is equal to the energy required for the electron to excite from its valence band to conduction band, each SWCNT will absorb light. These peaks are assigned to Van Hove singularities, which are observed when individual or bundled SWCNTs are present in the solution. [26]

The absorption spectrum is classified into 4 regions corresponding to different absorption bands. The absorption bands in the range of 340nm-400nm, 850-1450nm and 500-850nm correspond to $E^s_{33,}$ $E^s_{11,}$ and E^s_{22} inter band electronic transition in the semiconducting tubes. Absorption band in a range of 420-520nm is due to electronic transitions in the metallic tubes $E^m_{11.}$ The absorption

in these transitions represents the length of the nanotubes irrespective of their concentration in the solution. [27]

3.6.2 Raman Spectroscopy

Raman spectroscopy is a technique widely used by researchers to characterize carbon nanotubes for their defects, (n, m) structure, diameter [28]. A strong mode of Raman spectra for SWCNTs was observed at 200cm^{-1} called the Radial breathing mode due to the radial vibrations of the tubes. Graphitic species show strong spectral lines around 1584^{-1} as globally known [34].

A Perkin Elmer Raman Micro series 785nm diode laser was used to characterize the CNTs. The exposure time was set to 3 seconds with 4 numbers of exposures and going at a magnification of 100x which leads to 1μm scan size of CNTs. The spectra of long, medium and short length CNTs is shown below in Figure 9.

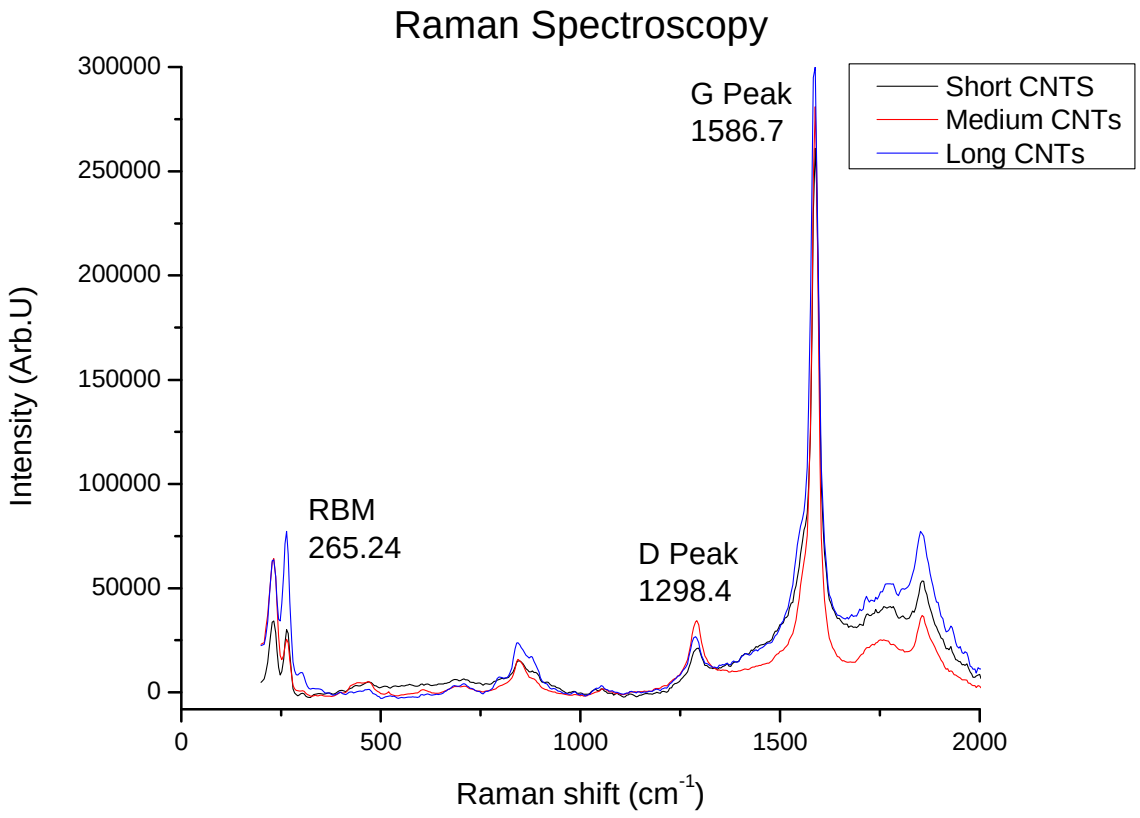

Figure 9: Represents Raman spectra of long, medium and short CNT fractions obtained from length separation process and dialysis

In the Raman spectra, a pre-dominant RBM and G peak were observed along with D peak. The appearance of D peak indicated the presence of side wall defects, which was considered as defects in CNTs. But here the high G: D peak ratio indicates that the CNTs are 95% defect free and there were no side wall defects. RBM peak gives the details of the diameter of CNTs.

3.6.3 Optical Microscope

An optical microscope was used to observe the wrinkling of PDMS at 50x magnification. Figure 10 obtained by one of our project mates Joseph Feeney, represents the 10% strained PDMS and 5% strained PDMS images which showed that the wrinkles obtained were very much close to each other. The wrinkling pattern reflects the membranes disordered mesostructure.

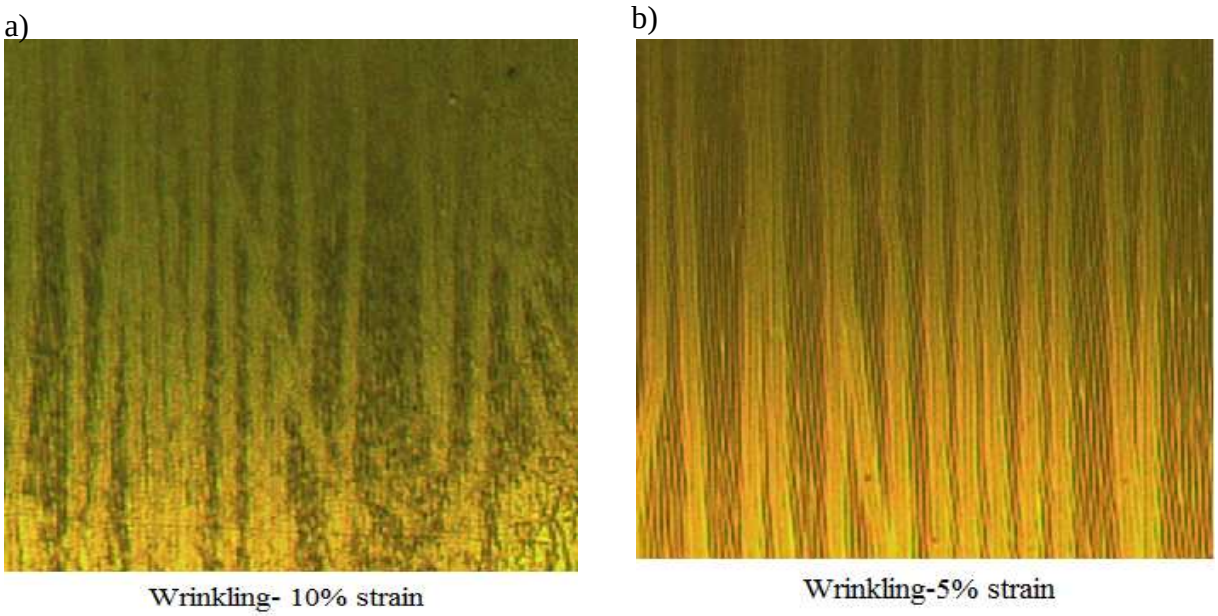

Figure 10: a) Represents optical microscope image of 10% strained PDMS and b) shows the optical microscope image of 5% strained PDMS

3.6.4 Scanning Electron Microscopy

Scanning electron microscopy is a high resolution powerful instrument for imaging and analyzing the nanoparticles. It gives the morphological information of the carbon nanotubes [36]. A Hitachi S-4700 Field emission scanning electron microscope was used to characterize CNTs. Here medium length CNTs sample was taken to observe their network connectivity and how well they were dispersed. Figure 11 shows the SEM images of medium length CNTs dispersed.

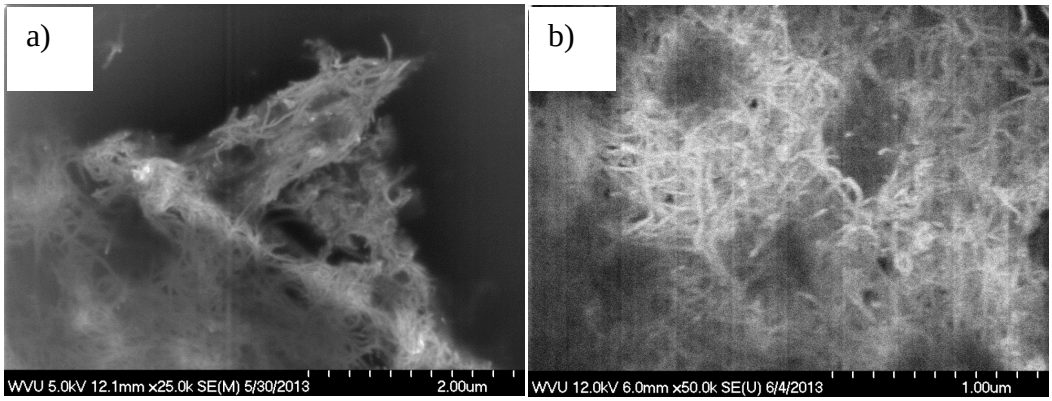

Figure 11: Represents SEM images medium length CNTs used as sensors in concrete samples

Figure 12 shows the images of wrinkled PDMS along with CNTs deposited on it. The wavelength of wrinkles of 10% strain on an average was measured to be 260nm and the wavelength of 5% strain was measured to be 285nm respectively. This showed that there was no much variation in the wrinkling PDMS of 5% and 10% strain.

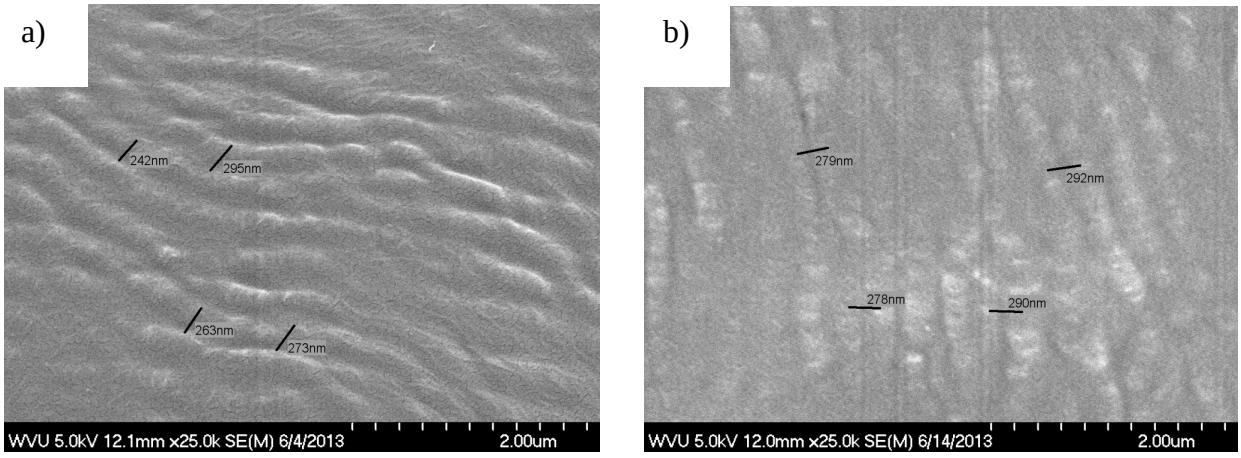

Figure 12: a) Represents SEM images of 10% wrinkled shorter length CNTs on PDMS substrate and b) used images of 5% wrinkled longer length CNTs on PDMS substrate as sensors in concrete samples

Calculations for finding the elastic modulus of SWCNTs are as follows

Elastic modulus of PDMS substrate, E_s = 1.8Mpa

Poisson's ratio of PDMS substrate, μ_s = 0.48

$$\bar{E}_s = \frac{E_s}{1-\mu_s^2}$$
$$= \frac{1.8}{1-0.48^2}$$
$$= 2.3389Mpa$$

Upon the release of pre-strain a homogenous film of thickness 'h' and modulus E_f develops a sinusoidal wrinkling pattern of wavelength, $\lambda_o = 2\pi h(\bar{E}_f/3\bar{E}_s)^{1/3}$

For 10% strained PDMS, λ_o=260nm and h = 3nm

Therefore $\bar{E}_f = 18.414Gpa$ and $\bar{E}_f = \frac{E_f}{1-\mu_f^2}$

Poisson ratio of SWCNT film is assumed to be 0.3 here.

Therefore, the Young's modulus of the SWCNT film is E_f = 16.757Gpa

For 5% strained PDMS, λ_o=285nm and h = 3nm

Therefore $\bar{E}_f = 24.253Gpa$ and $\bar{E}_f = \frac{E_f}{1-\mu_f^2}$

Poisson ratio of SWCNT film is assumed to be 0.3 here.

Therefore, the Young's modulus of the SWCNT film is E_f = 22.07Gpa

3.6.4 Atomic force microscopy

The atomic force microscopy is widely used for the three dimensional topographic images of the nano-materials with atomic resolution for short time. AFM is used for analyzing the morphological information of the nanostructures [37].

A Veeco multimode Scanning probe microscopy (AFM) was used to determine the CNTs length. One of our research group student's Sai Gunturu has worked on AFM and found out that the fraction 9, fraction 11 and fraction 14 had lengths of 879 nm and medium 340-400nm and short to be 220nm. Figure 12c shows the longer length CNTs on silicon substrate and its length was measured to be 879nm.

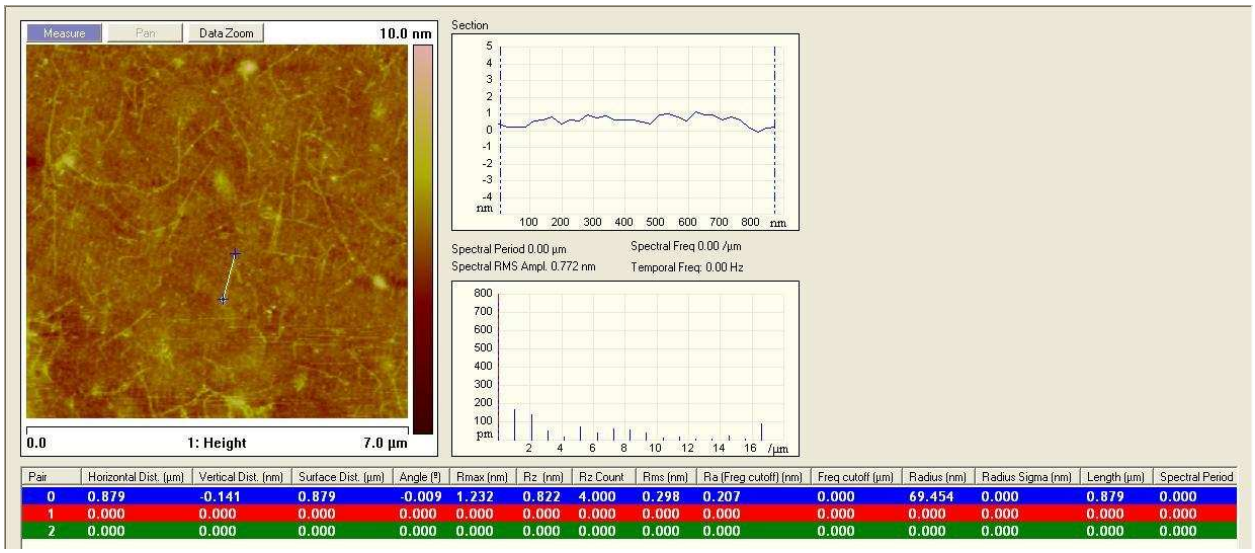

Pair	Horizontal Dist. (µm)	Vertical Dist. (nm)	Surface Dist. (µm)	Angle (°)	Rmax (nm)	Rz (nm)	Rz Count	Rms (nm)	Ra (Freq cutoff) (nm)	Freq cutoff (µm)	Radius (nm)	Radius Sigma (nm)	Length (µm)	Spectral Period
0	0.879	-0.141	0.879	-0.009	1.232	0.822	4.000	0.298	0.207	0.000	69.454	0.000	0.879	0.000
1	0.000	0.000	0.000	0.000	0.000	0.000	0.000	0.000	0.000	0.000	0.000	0.000	0.000	0.000
2	0.000	0.000	0.000	0.000	0.000	0.000	0.000	0.000	0.000	0.000	0.000	0.000	0.000	0.000

Figure 13: c) Represents AFM image of longer length CNTs

Chapter 4

MATERIAL PROPERTIES

4.1 Concrete

Concrete generally composes of paste and aggregates, where paste forms a combination of Portland cement and water and coats the surface of fine and coarse aggregates. The paste hardens and gains strength to form hard material known as concrete through a chemical reaction called hydration. To achieve a strong and durable concrete, proportioning and mixing concrete plays an important role. These properties of concrete are the reason behind the concrete being used for building skyscrapers, houses, dams, bridges, pipelines and sidewalks. In our research, concrete is being used as the base matrix for which the defects can be identified using CNT-smart materials [4, 35].

4.1.1 Concrete design

A well designed concrete mixture comprises of 10-15% cement, 60-75% aggregate and 15-20% water and air may also occupy 5-8%. [29]

Portland cement: The type of cement used in this experiment is the Saylor's Portland cement type I/II purchased from Essroc Cement Corp conforming to ASTM C150, ASTM C1157, and AASHTO M-85. This type I/II is a general purpose cement that is most commonly used as it gives excellent results in wide range of applications and offers resistance to sulphate attack and provides low heat generation. [29]

Table 1: Main constituents of Portland cement [29]

Chemical Name	Chemical Formula	Shorthand Notation	Percent by Weight
Tricalcium Silicate	$3CaO.SiO_2$	C_3S	50
Dicalcium Silicate	$2CaO.SiO_2$	C_2S	25
Tricalcium Aluminate	$3CaO.Al_2O_3$	C_3A	12
Tetracalcium Aluminoferrite	$4CaO.Al_2O_3.Fe_2O_3$	C_4AF	8
Gypsum	$CaSO_4.H_2O$	CSH_2	3.5

Chemical compound constituents of Portland cement when mixed with water undergo a series of chemical reactions called hydration. These reactions determine the strength and hardness of cement.

Aggregate: This comprises of sand, gravel and crushed stone which in turn is combined with a binding medium called Portland cement and water to form rock-like structure called concrete [29]

Aggregates are taken from either natural or manufactured sources. Natural aggregates come from three broad geological classifications called igneous rock, sedimentary rocks and metamorphic rocks. Manufactured rock is formed from the industrial byproducts slag produced when steel, tin or copper were in production. The type and size of the aggregate mixture depends on the final concrete product.

In our research Sakrete All purpose sand called the crystalline silica (quartz) SiO_2 was used. Its specific gravity ranges from 2.5-2.8.

Water: Excessive impurities when mixing water with cement and aggregate may affect concrete strength and setting time. It may also affect the corrosion of reinforcement and reduces its durability [29]. Drinking water or de-ionized water has been used in our experiment to maintain the quality of sample.

4.2 Sodium De-oxycholate

De-oxycholic acid soluble in water, forms molecular co-ordination compounds with many substances. DOC ($C_{24}H_{39}O_4Na$) is a surfactant used in dispersing and bundle defoliating CNTs. In our experiment, we followed Density gradient Ultracentrifugation technique for sorting the SWCNTs according to their length. DOC dispersed SWCNTs were length sorted via DGU. DOC for our work is purchased from Sigma Aldrich.

4.3 Opti-Prep density gradient medium

The Opti-prep Density gradient medium is a 60% (w/v) solution of iodixanol in water. The main function of DGU is to separate CNTs either by their buoyancy density or their rate of sedimentation.

4.4 Poly Di-methyl Siloxane (PDMS)

In order to wrinkle the SWCNTs, pre-strained PDMS $(C_2H_6OSi)_n$ strips were used as the substrates. The preparation of PDMS comprises of mixing SYLGARD ® 184 Silicone Elastomer base and SYLGARD ® 184 Silicone Elastomer curing agent in the ratio 10:1 and allowing it to cure 24 hrs.

Table 2: Properties of PDMS [30]

Tensile strength	1022psi
Elongation (% at break)	113%
Viscosity 25degc	5004.09 cSt

4.5 Polystyrene

Polystyrene in pellet form of molecular weight 192,000 was purchased from Sigma Aldrich. In our experiment spin coated polystyrene films were important in transferring wrinkled CNTs.

4.6 Other Solvents

Isopropanol: Isopropanol purchased from Fischer Scientific was in used in the sample preparation of CNTs for SEM and AFM

Acetone: Acetone purchased from Acros Organics was in used in the sample preparation of CNTs for SEM and AFM

Toluene: Polystyrene films were prepared by dissolving P.S pellets in Toluene ($C_6H_5CH_3$). For our experiment Toluene for purchased from Fisher Scientific

Methanol: Methanol purchased from Fischer Scientific was in used in the sample preparation of CNTs for SEM and AFM

Chapter 5

EXPERIMENTAL SETUP

5.1 Introduction

Environmental deterioration, chemical reaction aging, shrinkage, thermal stress, corrosion, externally applied loads, poor construction practices, construction overloads, and errors in design are the reasons for the failure of cement based structures through formation of cracks [2, 3]. Sensitivity of detecting the micro-cracks will be affected by varying the nanotube lengths and simultaneously by the wavelength of wrinkles [12].

The strength of concrete is the important factor to be known which can be determined through bending, shear and compression tests. Curing of the concrete plays an important role for the structure in gaining compressive strength [39]. When the sample is tested in bending conditions, it breaks at a point indicating its failure due to bending. In order to identify the cracks at the initial stage, a carbon nanotube sensor was embedded in the concrete and thereby the change in impedance was measured by an impedance analyzer.

5.2 Sensor fabrication

The CNTs used for this experiment are the South West Nanotechnologies CG100 single wall carbon nanotubes. These SWCNTs diameter varies in the range of 0.87±0.3 nm and has a high aspect ratio of 1150. They are consistent in Chirality distribution, have good electrical conductivity and have high purity [31]. Since, these CNTs were varied length wise and were bundled; they were subjected to ultra-sonication followed by density gradient ultracentrifugation to break the bundles and sort the CNTs according to length. To confirm this, we used different characterization instruments such as the UV-Vis-NIR Spectroscopy, Raman spectroscopy, Atomic force Microscopy (AFM) and the Scanning electron microscopy (SEM). From the above mentioned characterization techniques, we concluded that we have used defect free nanotubes, well separated from bundles, sorted and grouped into 3 groups namely long CNTs (1μm-800nm), medium CNTs (600-400nm), short CNTs (<300nm) and diameter of CNTs ranging from (0.5-1.2nm). These homogenous length sorted SWCNT thin films were subjected to varying strain conditions in order to obtain unique wrinkling SWCNT meshes. These wrinkled meshes were

embedded into concrete samples which in turn were subjected to bend test and the impedance measured across the sample gave the details of defects.

Table 3: Types of concrete samples prepared

Type	Nanotube layer	Toluene	Dimensions of the CNT layer
Type 1	Absent	Absent	-
Type 2	Absent	Present	-
Type 3	Present	Present	2.54x2.54cm^2

All the type 1, type 2, type 3 samples were designed according to the ASTM standards and they were subjected to the 3 point loading test and the impedance across the samples were taken at every load. All the impedance results of the type 1, type 2 and type 3 samples were compared and discussed in the following sections.

5.3 Test specimen overview

5.3.1 Type 1: Mortar samples

The specimen of dimensions 7.5x2.5x2.5cm^3 was prepared for this study. The specimen consists of mixture of cement, sand and water. Here the quantity of cement required is 1 part by mass, sand 2.75 parts by mass, and water 0.45 parts by mass. Figure 14, shows the mortar sample used in experiments.

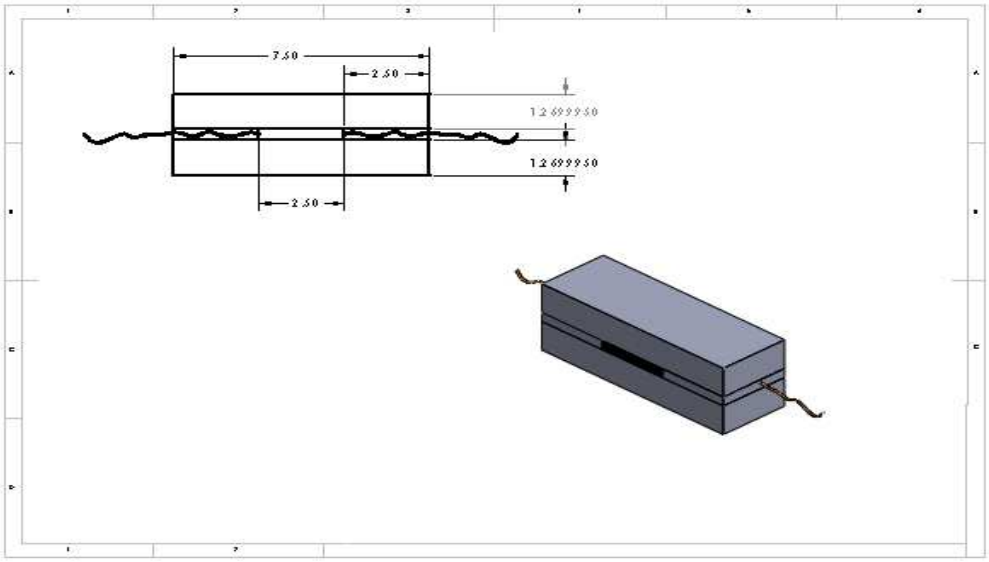

Figure 14: Represents SWCNTs embedded concrete sample overview with front view and isometric view, dimensions in cm

5.3.2 Type 2: Mortar samples containing toluene

Specimens of dimensions 7.5x2.5x2.5cm^3 were prepared for this study. The specimen consists of mixture of cement, sand and water and toluene. Here the quantity of cement required is 1 part by mass, sand 2.75 parts by mass, and water 0.45 parts by mass. The weight percentage of toluene added to the samples is 0.128% and it is the amount required to dissolve the polystyrene film.

5.3.3 Type 3: Concrete samples containing wrinkled SWCNT meshes

Specimens of dimensions 7.5x2.5x2.5cm^3 were made for this study. Specimens were divided into 3 layers in which layer 1 and layer 3 consists of mixture of cement, sand and water and layer 2 consists of wrinkled SWCNT meshes transferred onto concrete by dissolving the polystyrene surface with toluene. Figure 13, gives the details of layers in concrete sample used in experiments.

Table shows the dimensions of the 3 layers in the concrete sample.

Table 4: The dimensions of different layers

Layer	Length (cm)	Width (cm)	Thickness (cm)
Layer 1	7.5	2.5	1.6666

Layer 2	2.5	2.5	10^{-6}
Layer 3	7.5	2.5	0.8333

Table 5: Content in each layer and weight percentage of CNTs in concrete samples

Layer	Cement (parts by mass)	Sand (parts by mass)	Water (parts by mass)	SWCNTs (w%)	Toluene (W%)
Layer 1	1	2.75	0.45	-	-
Layer 2	-	-	-	0.1078	0.128
Layer 3	1	2.75	0.45	-	-

For all the three types of samples, two copper wires having 1 cm apart were inserted from both ends at a distance of 1/3rd from the base for the measurement of impedance across the sample. These wires were placed 1cm apart and they connect the wrinkled SWCNT meshes in type 3 sample. The copper wires were clipped to the alligator clips of the impedance analyzer to measure the impedance while the load being applied upon the sample.

5.4 Procedure for samples preparation

5.4.1 Type 1 sample - mortar

The quantity of cement, sand and water required for making a mortar sample were weighed and taken into a dovetail mixing apparatus. To get a better mixture, the lumps in the cement should be grinded off first, then the sand is added to cement and both were mixed thoroughly. Water is added little by little to the mixture and the mixture was mixed thoroughly for 30s at slow speed nearly 140r/min and then for 30s at 280r/min using a dovetail mixer.

Acrylic Plexiglas sheets were used in machining the molds according to the dimensions (±0.05cm and 90±0.5º geometric tolerance) shown in solid works software. The molds were assembled carefully and the walls were perfectly held in 90º inclination with other walls. Even before filling the molds with the mortar mixture, it was ensured that the walls have been degreased for the easy removal of sample from the molds after 24 hours of sample preparation. The obtained mixture was then filled into the mold up to 1/3rd layer from the bottom. Copper

wires which were bent into L shape were inserted from both ends at a distance of 1cm apart at the center. Again the mixture was filled and rammed thoroughly to avoid air pockets in the mold. Six samples of mortar were prepared and were tested on the 14th day of the curing. Figure 15 shows the image of the mold used for sample preparation.

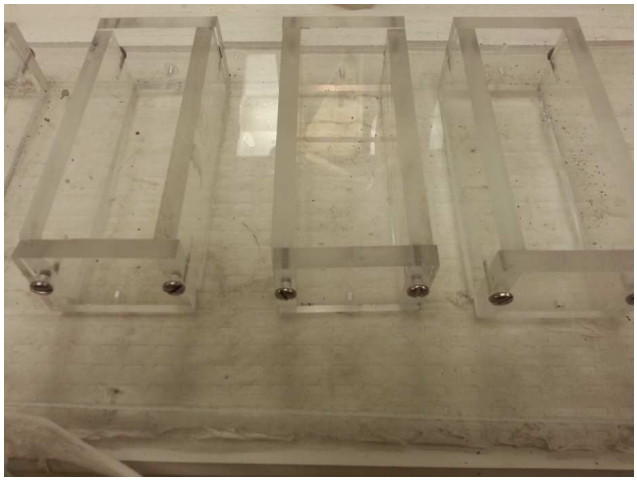

Figure 15: Shows the image of mold for making SWCNTs embedded concrete sample

5.4.2 Type 2 sample – Toluene added to mortar

In this type of sample, toluene was added to the mortar mixture after mixing the cement, sand and water contents. The amount of toluene added to the sample was the amount required to dissolve the polystyrene film, which acted as a substrate in transferring the wrinkled CNTs, discussed in later sections. This sample was prepared in order to study the affect of adding toluene to the mortar mixture.

The procedure for mixing the mortar contents was repeated just as told in section 5.4.1. Toluene was added to this mixture and then the mixture was again mixed thoroughly prior to filling the molds. The procedure described in section 5.4.1 was followed for pouring this mixture into molds. Six samples of this type of sample were prepared and were tested on the 14th day of curing.

5.4.3 Type 3 sample – Wrinkled SWCNT mesh and toluene added to mortar

This sample consists of 3 layers as mentioned in section 5.3.3. Layer 1 and layer 3 together make sample of type 1 for which the procedure was already mentioned in section 5.4.1. For sample of

type 3, we need to focus on obtaining surfactant free wrinkled SWCNTs to embed into mortar sample. After the DGU length sorting process of SWCNTs, homogenous length sorted fractions of SWCNTs remained along with sodium de-oxycholate (surfactant), and a density gradient opti-prep solution. To remove these excess salts, a process called dialysis was done to obtain length sorted chemical free SWCNTs. This process of dialysis is discussed in 5.4.3.1 in detail.

Our project concentrated on studying the affect of various strain rate of wrinkling the length sorted CNTs. Wrinkling of CNTs was done using a strain stage which was designed using solid works. Figure 16 shows the model of a strain stage for wrinkling the CNTs.

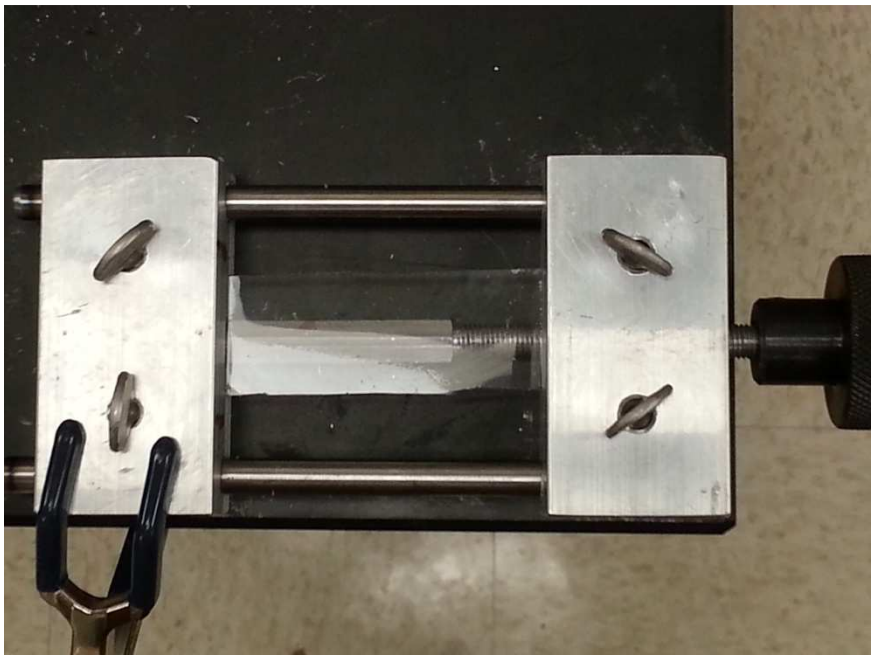

Figure 16: Shows the image of strain stage for wrinkling SWCNTs embedded in concrete sample

5.4.3.1 Sample preparation protocol

The following were the steps involved in preparing the length fractionated wrinkled SWCNT films:

Dialysis of SWCNTs solution

Dialysis was used to remove the surfactant and the density gradient from length sorted SWCNTs solution which was in turn used in creating 2D networks of SWCNTs. Figure 17 shows the dialysis equipment used in the laboratory.

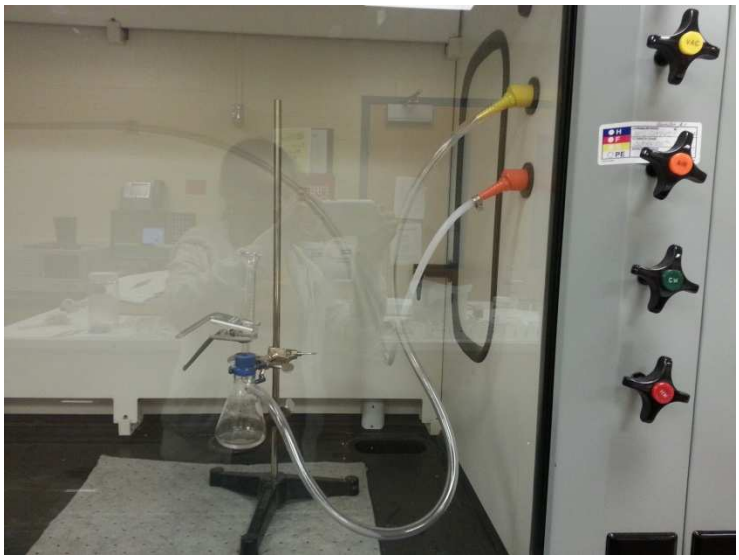

Figure 17: Shows the image of dialysis technique for obtaining salt free SWCNTs embedded in concrete sample

SWCNTs fractions obtained after DGU length sorting technique contains a surfactant called Sodium de-oxycholate and a density gradient “optiprep solution”. To get rid of these chemicals, the SWCNTs solution was poured along with a mixture of isopropanol and DI water (ratio 1:4) in the ultrafiltration cell in which 0.05μm VMWP membrane filter, purchased from Millipore was placed. Then the ultrafilter was then placed on Fisher scientific isotemp digital magnetic stirrer and constant air was supplied to the ultrafiltration cell. This created a constant atmospheric pressure which drove away the excess solution containing the chemicals out of the cell leaving SWCNTs solution in the cell.

Vacuum filtration

Vacuum filtration process was used to collect the length sorted SWCNTs deposited on the surface of a porous cellulose ester membrane. SWCNTs solution obtained after dialysis process was poured into a funnel which passes through a membrane. A mixture of Isopropanol and DI water in the ratio 1: 4 was added and vacuum was applied to rinse away any remaining Sodium deoxycholate present in the solution. This retained the CNTs and the filtrate was collected into another flask, directly or via a vacuum manifold.

Preparation of PDMS

Polydimethyl Siloxane (PDMS) was prepared by mixing the silicone elastomer base and the silicon curing agent in a 10: 1 ratio. The mixture was poured into petri dishes and was cured at room temperature overnight and left on a table. Now the Poisson's ratio and the elastic properties of the PDMS were calculated easily.

Preparation of polystyrene films

Polystyrene films were made by spin coating polystyrene solution on 1" x 1" cut silicon wafers. A spin coater model P6700 series was shown in Figure 18. This polystyrene solution was obtained by dissolving polystyrene pellets having molecular weight 192000 in toluene in 1:4 parts by mass. These PS films were floated off the silicon wafers in a beaker of DI water. The protocol for spin coating is discussed in later sections.

Figure 18: Shows a spin coater for spinning polystyrene to make PS films

Wrinkling length sorted SWCNTs thin films

PDMS strips of dimensions 7.5x2.5x0.5cm^3 were cut using a mold and placed onto a strain stage, which was used to apply a pre-strain to the samples obtained. A known pre-strain was applied to PDMS strip prior to placing the PS film on it. Length sorted SWCNT thin film deposited on the cellulose membrane obtained via vacuum filtration process was adhered to PS film. The strained PDMS along with PS layer adhered to length sorted SWCNT film deposited on a cellulose membrane was released to induce in plane wrinkles unique to the length and strain of CNTs.

The PS layer served as a removable layer between the PDMS and the wrinkled SWCNT mesh which was easily transferred on to the concrete sample. Toluene dissolves this PS layer leaving the length sorted SWCNT wrinkled mesh called the layer 2 on the layer 3 of the concrete sample. The copper wires were placed connecting the SWCNT mesh and layer 1 was filled with remaining concrete mix.

5.5 Calculations made for Samples preparation

5.5.1 Sample preparation of Mortar

Mortar sample made for our study consisted of cement, sand and water. The following were the calculations made in the preparation of mortar sample.

Dimensions of the mortar block are as follows:

Length = 7.5cm
Width = 2.5 cm
Thickness or Height = 2.5 cm
Therefore the volume of the block = L x W x H

= 7.5 x 2.5 x 2.5

= 46.875 cm^3

Concrete mix contains cement, sand and water in the ratio of 1: 2.75: 0.45 parts by mass. So the mass of cement, sand and water required for a perfect concrete mix are calculated using equation

$$\frac{x}{3.15} + \frac{2.75x}{2.68} + \frac{0.45x}{1} = 46.875$$

Where, x is the mass of the cement in 'grams'

'3.15' is the specific gravity of the Portland cement

'2.68' is the specific gravity of the sand used

'1' is the specific gravity of water

'46.875' is the volume of the block in cm^3

Therefore, the obtained mass of the materials used to build concrete sample:

Cement (x) = 26.016 grams

Sand (2.75x) = 74.083 grams

Water (0.45x) = 11.707 grams

These quantities were mixed as told in section 5.4.1 and poured into molds and six samples were prepared to test on the 14^{th} day of curing.

5.5.2 Sample preparation of Mortar containing toluene

The entire composition of this type of sample included the constituents of mortar sample with toluene added to it. The amount of toluene added to the sample was the amount required to dissolve the 1" x 1" PS layer. The amount of toluene required to dissolve was 300µL which was measured to be 0.06grams by mass. This was 0.128% of weight of entire sample constituents.

The remaining calculations were same as 5.5.1. Six samples of this type were made and tested on the 14th day of curing.

5.5.3 Sample preparation of Mortar containing wrinkled SWCNT mesh and toluene

The entire composition of this type of sample also included the constituents of mortar sample with PS layer having winkled SWCNT mesh and toluene added to dissolve away the PS layer.

5.5.3.1 Spin coating PS protocol

Polystyrene pellets of molecular weight 192000 purchased from Sigma Aldrich were dissolved in toluene in 1:4 ratio of parts by mass to get a PS solution for spin coating. A silicon wafer was cut into 1" x 1" pieces each was initially air blown and then cleaned in an acetone bath. A spin coater of model P6700 was used and the Si wafer was placed on the spin coater and PS solution was poured onto it was spun at the following speeds for 3 runs to obtain a PS layer of thickness 37.5μm.

Table 6: Spin coating PS analysis

Speed (RPM)	Ramp (seconds)	Time (seconds)
250	3	30
1200	3	30

Silicone elastomer base of 40grams was mixed with the silicon curing agent of 4 grams, poured into petri dishes and was cured for 24 hours. The obtained PDMS membranes were 0.5cm thick.

Mortar constituents and composition remained same as 5.5.1 and 5.5.2 for this type of sample also. Six concrete samples having embedded with wrinkled long, medium and short SWCNT meshes of 10% strain and 5% strain each were made and tested on the 14th day of curing.

5.6 Curing

All types of samples prepared for this test were allowed to set in the molds for a period of 24 hours. The samples were taken out of the molds after 24 hours and were immersed in water bath for 4 days, 8 days and 12 days for gaining enough strength. The samples were allowed to dry in ambient conditions after taking out from the water bath. The impedance readings of all samples were taken for every 24 hours till the day of testing and were analyzed.

5.7 Three point bending

A three point bending test was done on the samples to see their strength and response of the CNTs during crack propagation while testing. Load was applied manually on the samples and it was ensured that it was applied perpendicular to the face of the sample without any eccentricity. The specimen to be tested was placed on the steel rollers (base) and below the cylindrical roller acting as a knife edge which was a load fixture as shown in Figure 19. Load was applied manually in 10 lbs increment and the impedance measurements across the specimen were taken after stabilizing for 3 seconds each time.

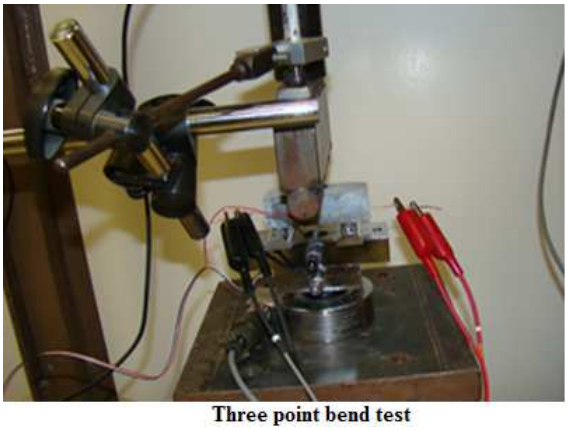

Three point bend test

Figure 19: Shows three point bend test equipment along with alligator clips of Impedance analyzer hooked to it to determine the impedance across the sample while loading

5.8 Sample Testing Procedure

Concrete mixture filled in the mold was allowed to set in for a period of 24 hours, there after all the samples prepared were immersed in a water bath for 4 days. The samples were taken out from the water bath after 4 days and were allowed to dry in ambient conditions. Impedance measured for each sample was taken for every 24 hours and compared. There was a steep increase in impedance from day 4 to day 6; then the impedance followed a linear pattern till the day 12 and later there was no much increase in the impedance. This shows that the sample did not hold any moisture and 12 days were sufficient for the sample to get dried.

5.8.1 Strain and Impedance measurement during static loading

Vishay Micro-Measurements system 5000 was used to measure the strain, displacement across the sample with respect to the loading conditions. A 4294A Agilent impedance analyzer was

used to monitor the impedance across the sample with respect to the strain developed in the sample during loading conditions.

For the strain measurement, a general purpose strain gages of grid resistance 350±0.3% in ohms were purchased from Micro-Measurements. These precision sensors were bonded to the bottom surface of the concrete using the M-Bond 200 adhesive kit purchased from the Vishay Micro-Measurements.

The following procedure was implemented to measure the impedance across the sample during the static loading conditions.

An attachment of 16089D alligator clip adaptor was fixed to 4294A impedance analyzer before power was supplied to the system. After turning on the equipment, it was allowed to initialize and then stabilize for 30 minutes as per given in the manual. The start frequency was set to 40Hz and the stop frequency to 220 KHz, the number of data points (sweep) was set to 801. The fixture compensation of the impedance analyzer was changed from “fixed mode” to “user mode” and the trigger was set to “continuous” in order to collect the data continuously.

To obtain precise and accurate results, a system calibration was done by performing an open and short circuit using the alligator clips and the charge between them was also nullified. Then a resistance of a standard resistor was measured and verified. The equipment was all set to take measurements of impedance after the calibration was done.

The impedance of all the three types of samples (type 1, type 2, and type 3) was monitored while subjected to bending test. The samples one after the other were placed between the spherically seated bearing block and the steel balls of the UTM.

The impedance analyzer software was installed on the computer which created a plug-in in Microsoft excel called 4395/4294A to collect the data. Three repeated measurements of impedance with an interval of 3 seconds were taken at zero loads initially. The load on the sample was incremented to nearly 10lbs and again an impedance measurement was taken. A cyclic process of loading was followed for every sample till it reached the breaking point (approximately 90lbs). Impedance across the sample was taken at every load and the change in impedance with respect to strain in the sample gives the details of micro-crack identification.

Chapter 6

RESULTS AND DISCUSSION

6.1 CNT sensors

CNTs of different lengths grouped under long, medium and short are identified and chosen from the 16 fractions obtained after centrifugation for fabrication of the sensors. Fraction 9, fraction 11, fraction 14 were picked up as long, medium and short CNTs as they have absorbance depending on their lengths with relatively similar concentration.

These concentrations were calculated from the absorbance values obtained from the UV-Vis-NIR Spectroscopy. The absorbance values taken at 775nm were used to calculate the concentration using Beer Lamberts law. The equation $A = \in CL$ represents Beer Lambert's law,

where, A - Absorption
$\in$ - Absorpvity
L - Length of the path of the cuvette

$\in$L is constant. Therefore, $\frac{A_1}{A_2} = \frac{C_1}{C_2}$

Here A_1 is the absorbance of the CNTs dispersed in Sodium De-Oxycholate of known concentration C_1= 1mg/ml

A_2 is the absorbance of the fractions 1-16 of CNTs, obtained from the UV-Vis NIR Spectroscopy and C_2 is the required concentration. Concentration of each fraction was calculated using equation from Beer-lambert's law [38].

Long - Fraction 9

$$\frac{0.44375}{0.08445} = \frac{1}{C_9}$$

$$C_9 = 1.903 * 10^2 \mu g/cm^3$$

Medium - Fraction 11

$$\frac{0.44375}{0.08445} = \frac{1}{C_{11}}$$

$$C_{11} = 1.918 * 10^2 \mu g/cm^3$$

Short - Fraction 14

$$\frac{0.44375}{0.08445} = \frac{1}{C_{14}}$$

$$C_{14} = 1.927 * 10^2 \mu g/cm^3$$

Figure 20 represents the graph plotted between absorbance and concentration of all the 16 fractions.

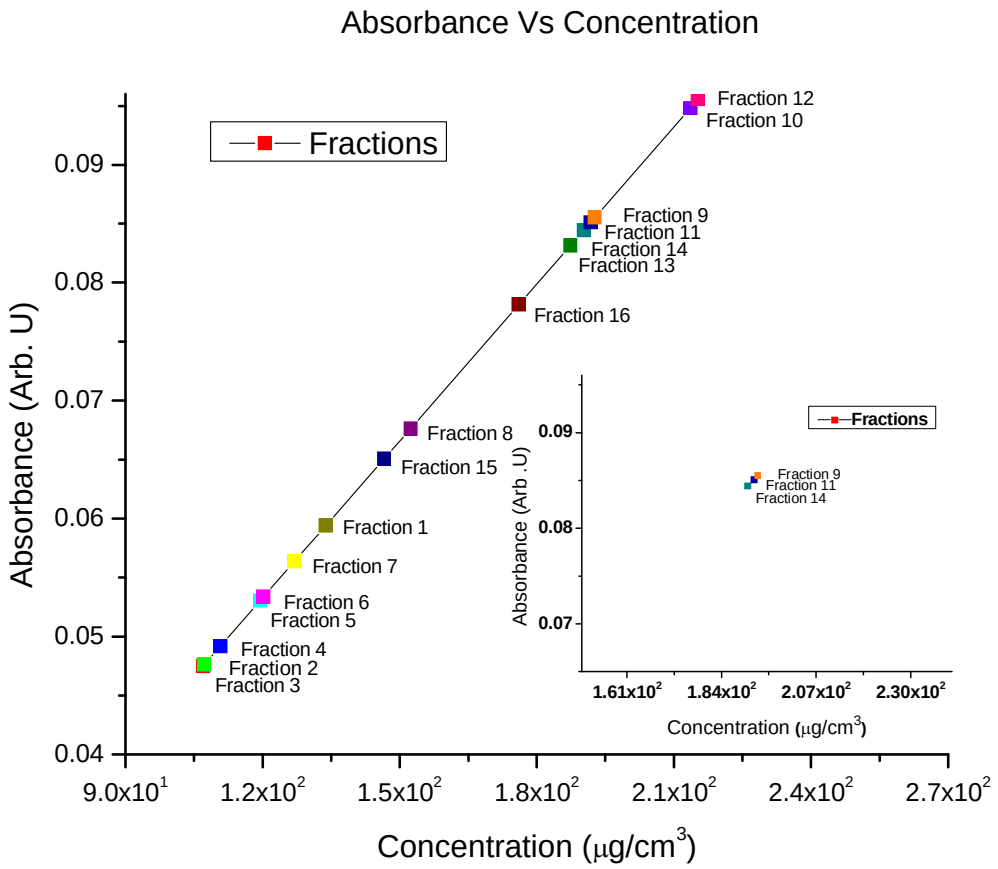

Figure 20: Optical absorbance as a function of concentration for length sorted CNTs obtained from UV-Vis-NIR spectroscopy

Three samples from each fraction were prepared with varied strain rate of wrinkling and were tested on the 14th day and their results were discussed in the following sections. This chapter mainly stresses on the application of using various strain rates of wrinkling length varied CNTs.

6.2 Impedance analysis during curing period

The concrete samples made of different length CNTs with varied strain rates were allowed to harden in the mold for 24 hours and then were submerged in a water bath for 4 days. In order to observe the change in impedance during curing period, the impedance across the concrete samples containing CNTs was monitored every day after taking those out from the water bath on the 4^{th} day.

Figure 21 represents the impedance of longer length, medium length and shorter length, 5% strained, wrinkled CNTs plotted as a function of time (days) in a logarithm scale. From the graph plotted, we inferred that the impedance across the samples was increasing from day to day which showed that the amount of moisture present in samples had completely vanished. These results prove that the impedance data obtained across the samples on the 14^{th} day test were free from the influence of moisture.

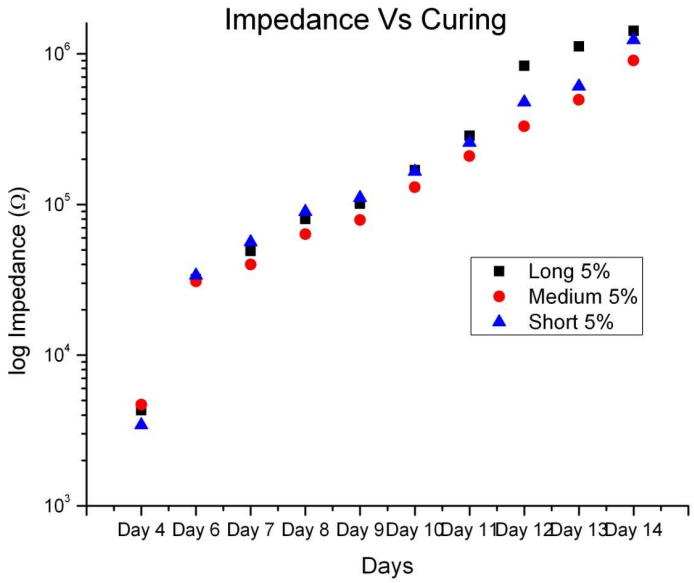

Figure 21: Represents impedance as a function of time (curing period) measured for longer, medium, shorter CNTs of 5% wrinkling

In Figure 22, the impedance of longer length, medium length and shorter length, 10% strained, wrinkled CNTs was plotted as a function of time (days) in a logarithm scale. From the graph plotted, we observed that the change in impedance increased with respect to the number of days passed which showed that it took 14 days for the samples to get dried and become free of moisture.

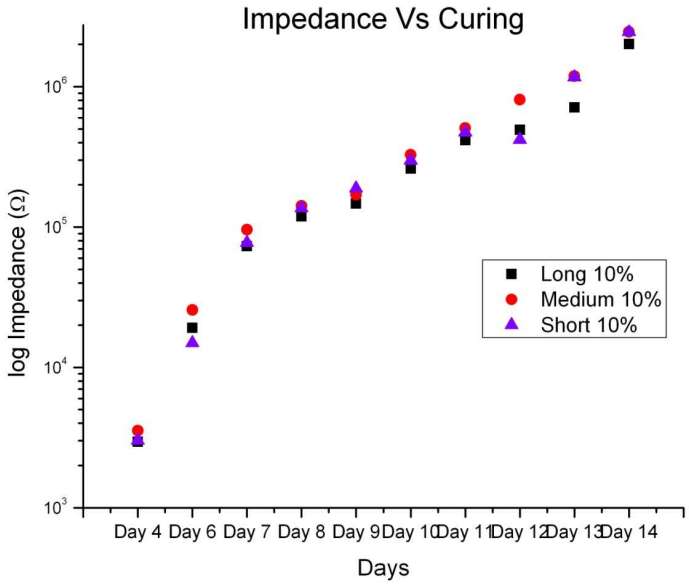

Figure 22: Represents impedance as a function of time (curing period) measured for longer, medium, shorter CNTs of 10% wrinkling

6.3 Impedance across the samples tested on 14th day

6.3.1 Impedance across the Mortar sample

The mixture of cement, sand and water that was filled in the mold was allowed to dry for 24 hours and later they were submerged in water. Six samples of this type were prepared and cured for 14 days and then tested. The impedance across the sample was measured at each point of load for three times in an interval of 3 seconds using Agilent impedance analyzer and the mean was plotted for the load values just before the sample broke. In order to observe the effect of moisture content present in the sample, we also varied another parameter known as the curing period. Curing is a process of hydrating the concrete samples so that the samples gain enough strength to

withstand loads and gaining strength of concrete depends on proper curing and time period. So the curing period of 4 days, 8 days and 12 days for each type of sample was plotted and the impedance data was taken for the 14th day bend test.

Figure 23 a. and 23 b. shows the plot of mortar sample cured for 8 days. This plot represents impedance and load as a function of strain. These two graphs show that the strain increases along with the increase in load and also an increase in the impedance with respect to increase in strain. This implies that the impedance increased as the crack started to propagate, according to Hou et al [11]. Since the curing process for these two samples was 8 days and as the drying of samples was not complete, the presence of moisture influenced the impedance readings and accounts for low absolute impedance values.

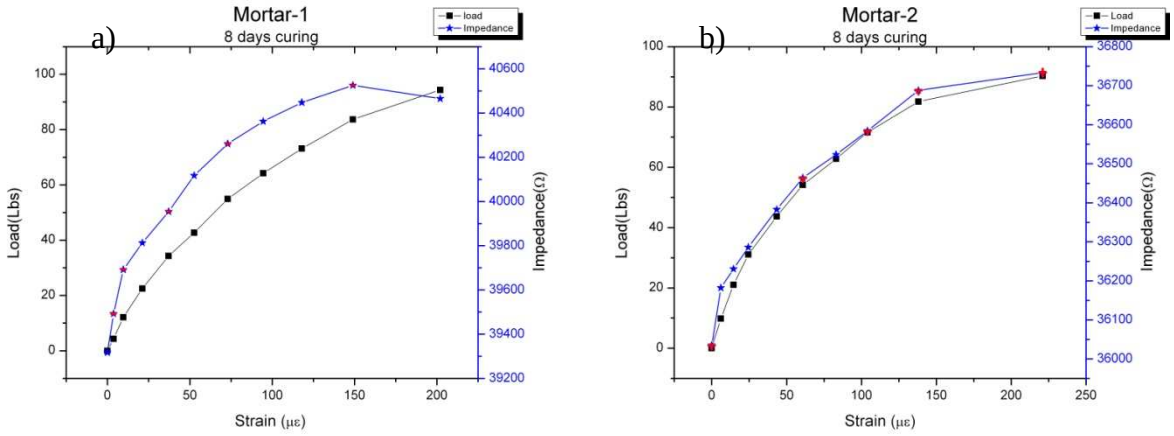

Figure 23: a. and b. Represents impedance and load as a function of strain for mortar sample cured for 8 days and tested on 14th day

Figure 24 shows the plot of mortar sample cured for 4 days. This plot represents impedance and load as a function of strain. This graph shows that the strain increases along with the increase in load but an increase followed by decrease in the impedance with respect to increase in strain. This implied that the impedance increases as the crack propagation starts but the decrease could be a reason of displacement of water pockets as this sample was under the process of getting dried. Since the curing process for this sample was 4 days and as the drying of samples was not complete, the presence of moisture was less when compared to 8 days and 12 days curing period the absolute impedance values were high.

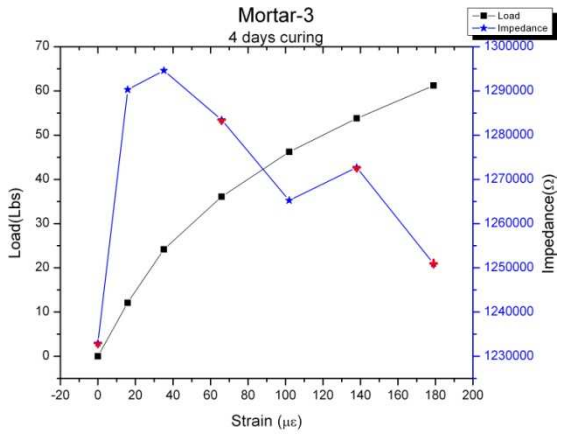

Figure 24: Represents impedance and load as a function of strain for mortar sample cured for 4 days and tested on 14th day

Figure 25 a. 25 b. and 25 c. shows the plot of mortar sample cured for 12 days. This plot represents impedance and load as a function of strain. These three graphs show that the strain increased along with the increase in load and also an increase in the impedance with respect to increase in strain. This implied that the impedance increased as the crack propagation started. Since the curing process for these three samples was 12 days and as the drying of samples was not complete, the presence of moisture influenced the impedance readings and accounts for lower absolute impedance values when compared to 4 days and 8 days curing period.

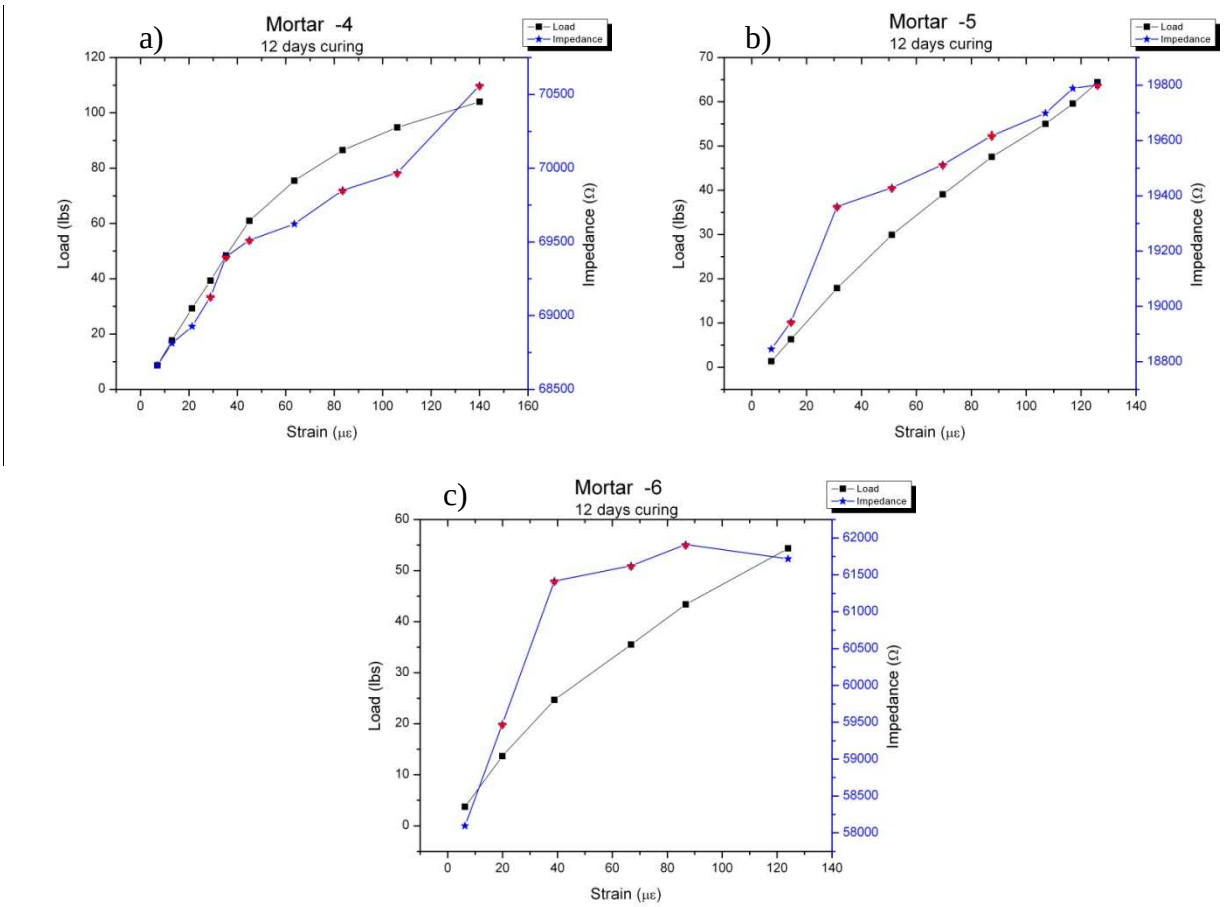

Figure 25: a. b. and c. Represents impedance and load as a function of strain for mortar sample cured for 12 days and tested on 14th day

From the data obtained after testing the six samples of mortar, it was observed that the influence of moisture resulted in variation of absolute impedance values but not the pattern of the plot. The co-efficient of variance reported in the data of each sample was less than 3% showing considerable repetition in data.

So, all the six curves of impedance were plotted in one graph with same scale to be compared with other samples data with the help of statistics. The impedance data of each sample was normalized by taking the least value as reference, but the obtained data still was in large scale which did not allow us to plot the curves in one graph under same scale. Then another step of taking percentage of all values with respect to maximum impedance was calculated and this scale obviously varied from 0 to 100 which made out task easier to plot all the data together.

Figure 26 represents the fitted curve of all the six samples of mortar plotted as percentage of maximum impedance being the function of strain. We used a polynomial curve fitting –degree 3 with equation $y = intercept + B_1x^1 + B_2x^2 + B_3x^3$. This curve fitting chosen was the best as it had 87.404% of R-square which represented the measure of fit. From this curve, it can be inferred that impedance increased as crack propagation developed till the sample broke.

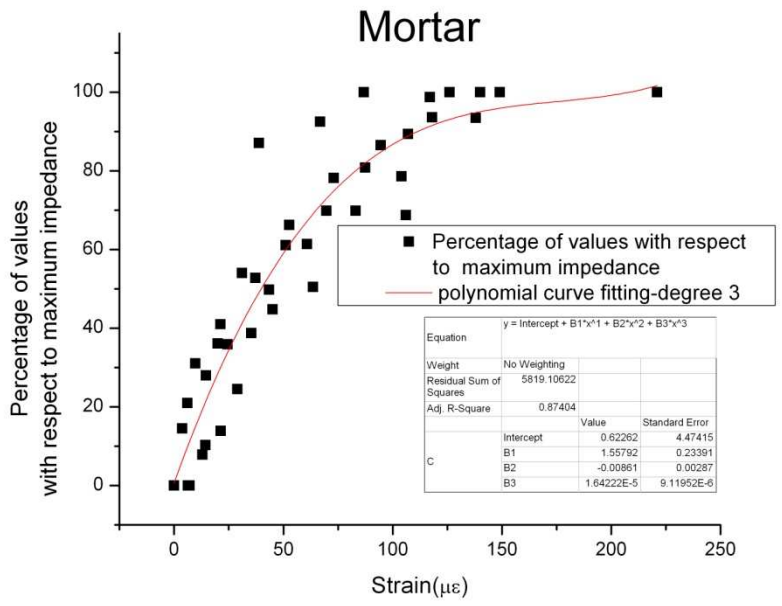

Figure 26: Represents the percentage of values with respect to maximum impedance as a function of strain (curve fitting plot) of the data of 6 mortar samples

6.3.2 Impedance across Mortar sample containing toluene

The mixture of toluene added to mortar was filled in the mold and was allowed to dry for 24 hours and later they were submerged in water. Same procedure as mentioned in section 6.3.2 was followed.

Figure 27 shows the plot of mortar sample containing toluene cured for 8 days. This plot represents impedance and load as a function of strain. These two graphs show that the strain increases along with the increase in load and also an increase in the impedance with respect to increase in strain. This implied that the impedance increased as the crack started to propagate. Since the curing process for these two samples was 8 days and as the drying of samples was not

complete, the presence of moisture influenced the impedance readings and accounts for low absolute impedance values.

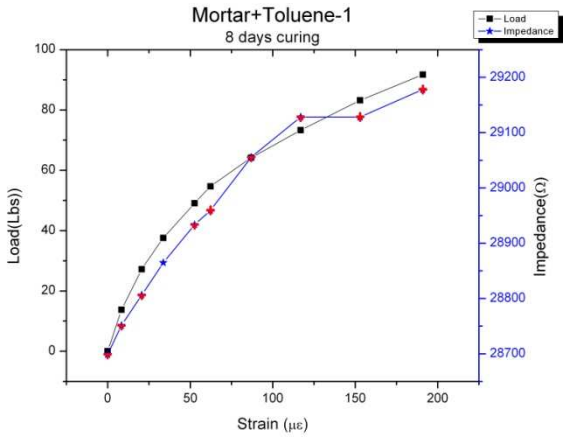

Figure 27: Represents impedance and load as a function of strain for mortar sample containing toluene cured for 8 days and tested on 14th day

Figure 28 a. b. shows the plot of mortar sample containing toluene cured for 4 days. This plot represents impedance and load as a function of strain. This graph shows that the strain increases along with the increase in load but an increase followed by decrease in the impedance with respect to increase in strain in one sample. This implied that the impedance increased as the crack propagation started but the decrease could be a reason of displacement of water pockets as this sample was under the process of getting dried. Since the curing process for this sample was 4 days and as the drying of samples was not complete, the presence of moisture was less when compared to 8 days and 12 days curing period the absolute impedance values were high.

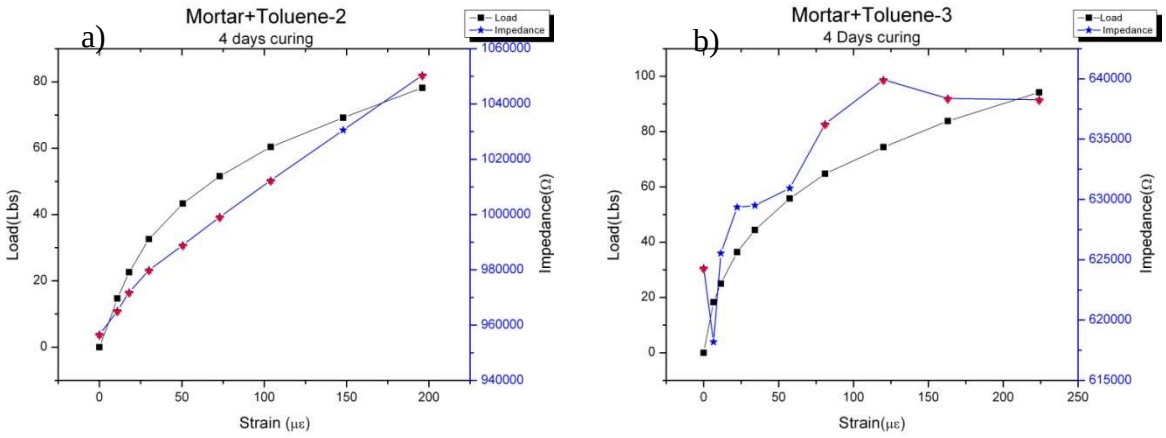

Figure 28: a. b. Represents impedance and load as a function of strain for mortar sample containing toluene cured for 4 days and tested on 14th day

Figure 29 a. 29 b. and 29 c. shows the plot of mortar sample containing toluene cured for 12 days. This plot represents impedance and load as a function of strain. These three graphs show that the strain increased along with the increase in load and also an increase in the impedance with respect to increase in strain. This implied that the impedance increases as the crack propagation starts. Since the curing process for these three samples was 12 days and as the drying of samples was not complete, the presence of moisture influenced the impedance readings and accounts for lower absolute impedance values when compared to 4 days and 8 days curing period.

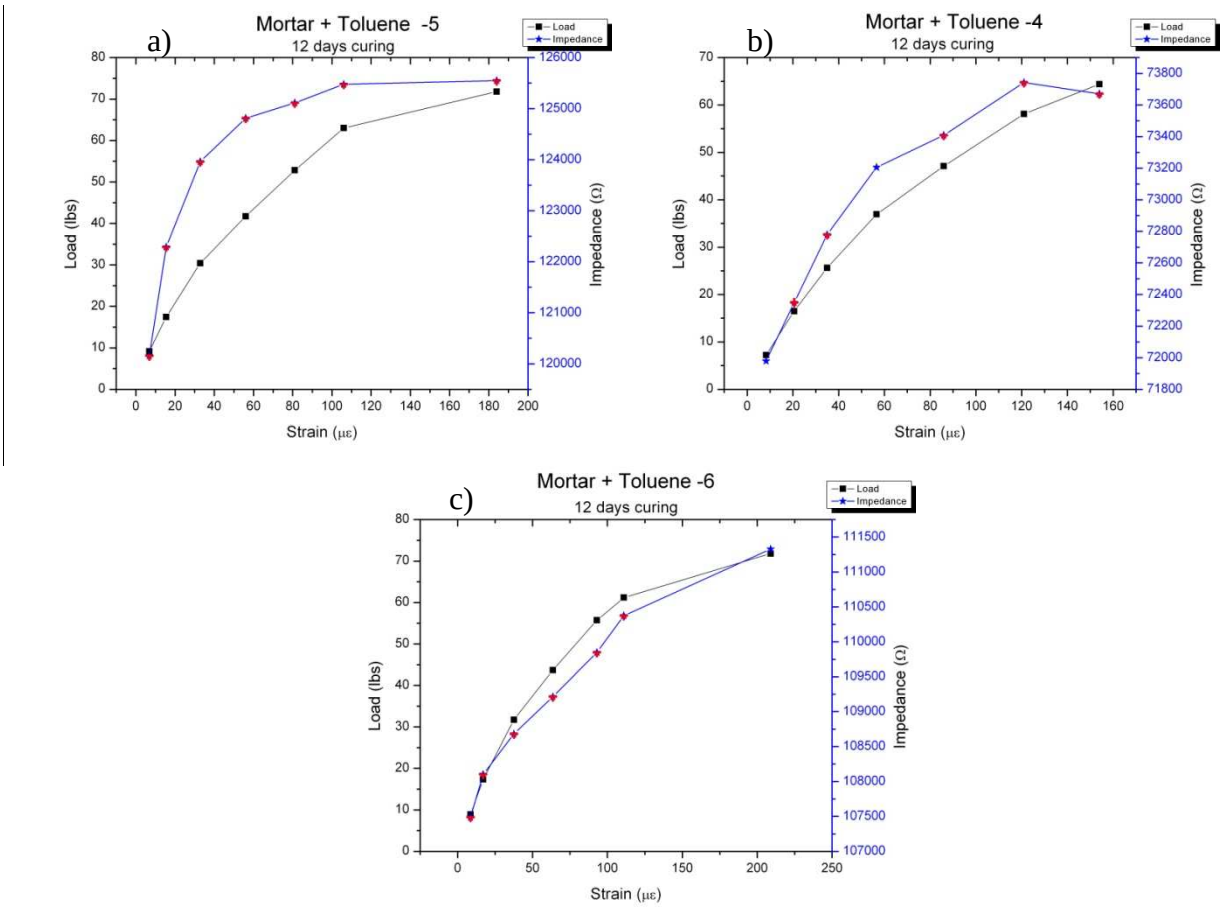

Figure 29: a. b. and c. Represents impedance and load as a function of strain for mortar sample cured for 12 days and tested on 14th day

Figure 30 represents the fitted curve of all the six samples of mortar plotted as percentage of maximum impedance being the function of strain. We used a polynomial curve fitting – degree 3 with equation $y = intercept + B_1x^1 + B_2x^2 + B_3x^3$. This curve fitting chosen was the best as it had 86.165% of R-square which represented the measure of fit. From this curve, it can be inferred that impedance increased as crack propagation developed till the sample broke.

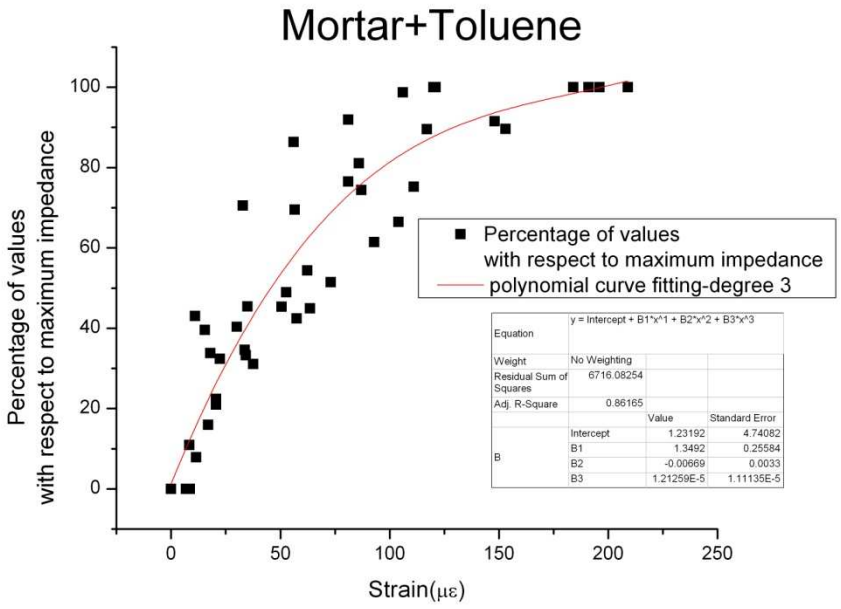

Figure 30: Represents the percentage of values with respect to maximum impedance as a function of strain (curve fitting plot) of the data of 6 mortar containing toluene samples

6.3.3 Impedance across concrete samples containing 10% wrinkled longer length CNTs

Concrete samples embedded with 10% strained longer length CNTs were cured in the mold for 24hours and later submerged in water. All the four samples made were tested on 14th day, with varied submerged period. Therefore, there was a variation in the absolute impedance values measured across each of the samples but the pattern of impedance for all the samples remained same according to the observed data.

The impedance across every sample was measured at each point of load for three times in an interval of 3 seconds and the mean was plotted till the load before sample failure.

Figure 31 shows the plot of 10% strained longer length CNTs embedded in concrete samples. The plots represent impedance and load as a function of strain.

Figure 31 a. b. shows data for samples cured for 8 days, here the strain increases along with the increase in load and also an increase in the impedance with respect to increase in strain. This implied that the impedance increased as the crack started to propagate. Since the curing process

for these two samples was 8 days and as the drying of samples was not complete, the presence of moisture influenced the impedance readings and accounts for low absolute impedance values.

Figure 31 c. shows data for samples cured for 4 days, here the strain increases along with the increase in load and then a pattern of huge increase and then decrease in the impedance with as the strain increased. This could be a sample of bad data misleading to any conclusions.

Figure 31 d. these graphs showed that strain increased along with the increase in load and also an increase in the impedance with respect to increase in strain. This implies that the impedance increases as the crack propagation starts. Since the curing process for these three samples was 12 days and as the drying of samples was not complete, the presence of moisture influenced the impedance readings and accounts for lower absolute impedance values when compared to 4 days and 8 days curing period. This data could not give any clue about the crack propagation.

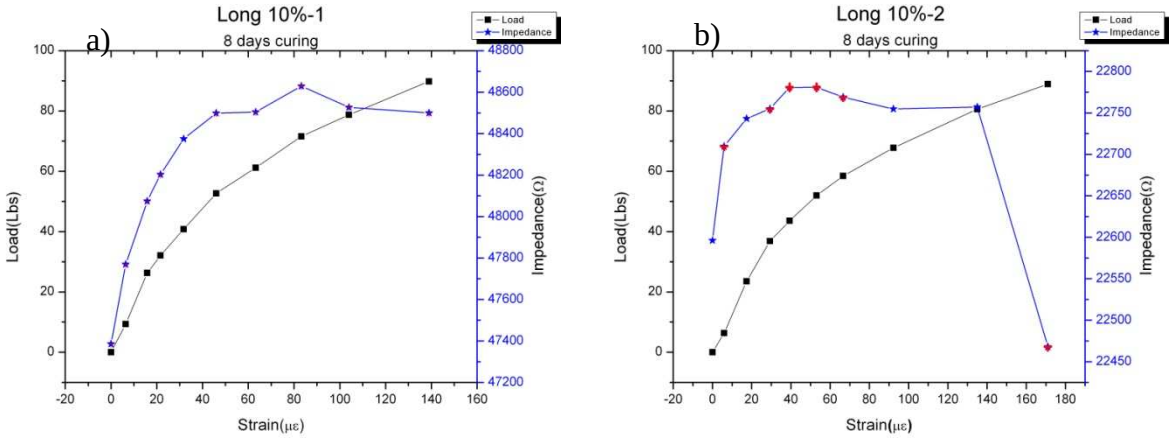

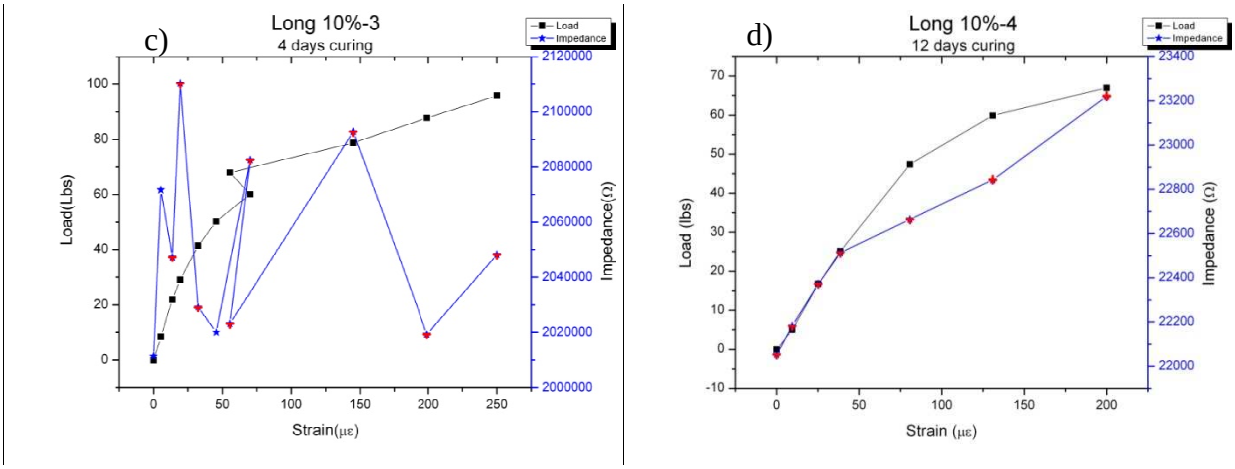

Figure 31: Represents impedance and load as a function of strain of the four concrete samples containing 10% strained longer length CNTs a), b) 8 days c) 4 days and d) 12 days curing period

Figure 32 represents the fitted curve of all the six samples of 10% strained longer length CNTs embedded concrete plotted as percentage of maximum impedance being the function of strain. We used an exponential curve with equation . This curve fitting chosen was the best as it had 53.538% of R-square which represented the measure of fit. From this curve, it can be inferred that impedance increased as crack propagation developed till the sample broke.

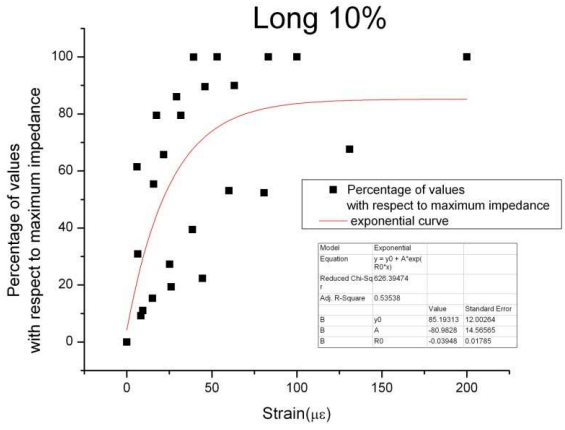

Figure 32: Represents the percentage of values with respect to maximum impedance as a function of strain (curve fitting plot) of the data of four concrete samples containing 10% strained longer length CNTs

6.3.4 Impedance across concrete samples containing 5% wrinkled longer length CNTs

Concrete samples embedded with 5% strained longer length CNTs were cured in the mold for 24hours and later submerged in water. All the four samples made were tested on 14th day, with varied submerged period. Therefore, there was a variation in the absolute impedance values measured across each of the samples but the pattern of impedance for all the samples remained same according to the observed data.

The impedance across every sample was measured at each point of load for three times in an interval of 3 seconds and the mean was plotted. The co-efficient of variance reported in the data was less than 3% showing a considerable repetition in the data. The results showed that impedance increased with propagation of micro-cracks.

Figure 33 a. b. shows data for samples cured for 4 days, here the strain increased along with the increase in load and also an increase in the impedance with respect to increase in strain.

Figure 33 c. d. represented graphs showed an increase in strain with the increase in load and a decrease in the impedance with increase in strain. This was a reason because of displacement of water pockets. Any conclusion basing on these samples cannot be made.

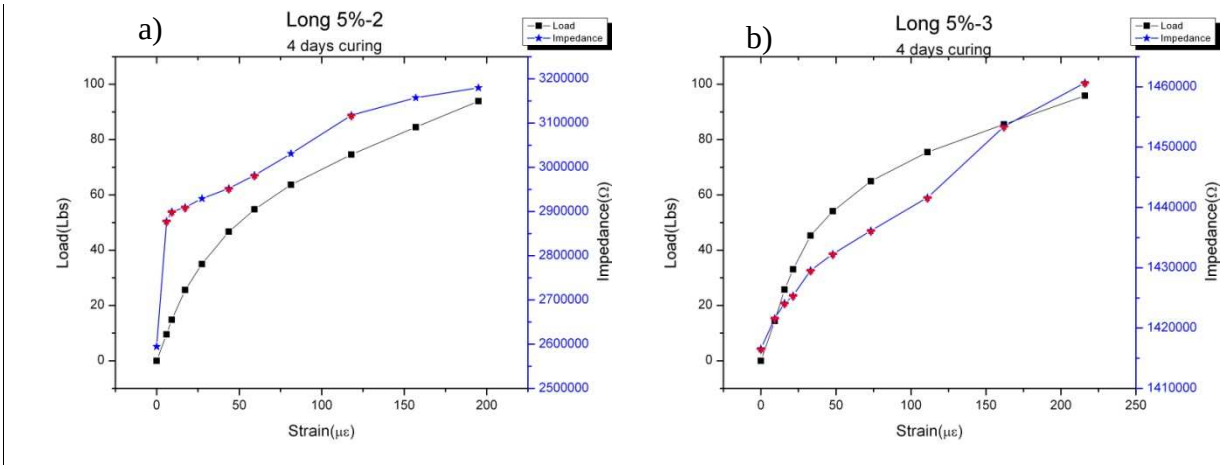

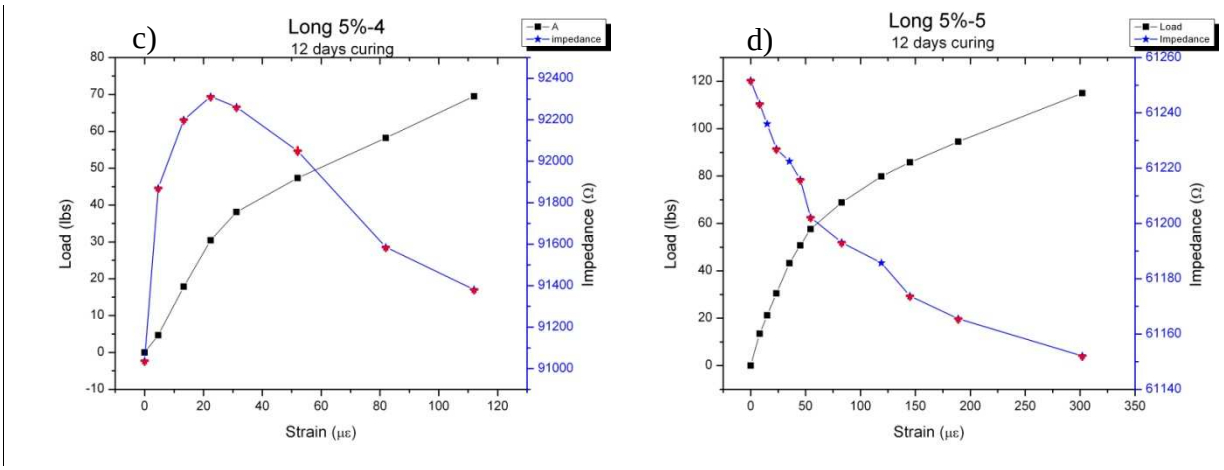

Figure 33: Represents impedance and load as a function of strain of the four concrete samples of 5% strained longer length CNTs a), b) 4 days c), d) 12 days curing period

Figure 34 represents the fitted curve of all the six samples of 5% strained longer length CNTs embedded concrete plotted as percentage of maximum impedance being the function of strain. We used an exponential curve with equation $y = y_o + A * \exp(R_o * x)$. This curve fitting chosen was the best as it had 38.325% of R-square which represented the measure of fit. From this curve, it can be inferred that impedance data obtained is not convincible to analyze or draw any conclusions from it.

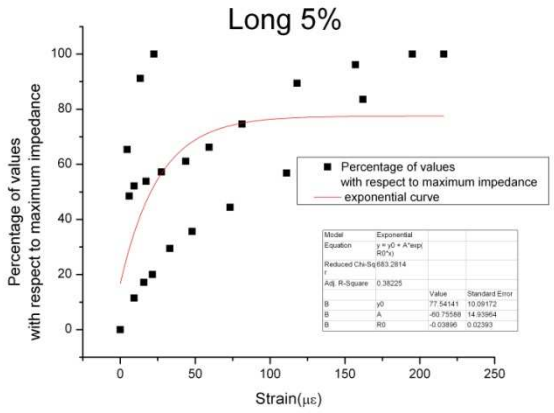

Figure 34: Represents the percentage of values with respect to maximum impedance as a function of strain (curve fitting plot) of the data of four concrete samples containing 5% strained longer length CNTs

6.3.5 Impedance across concrete samples containing 10% wrinkled medium length CNTs

Concrete samples embedded with 10% strained medium length CNTs were cured in the mold for 24hours and later submerged in water. All the six samples made were tested on 14th day, with varied submerged period. Therefore, there was a variation in the absolute impedance values measured across each of the samples but the pattern of impedance for all the samples remained same according to the observed data.

The impedance across every sample was measured at each point of load for three times in an interval of 3 seconds and the mean was plotted. The co-efficient of variance reported in the data was less than 3% showing a considerable repetition in the data. The results showed that impedance increased with propagation of micro-cracks.

Figure 35 a. c. and f. represent that there was a change in impedance with respect to crack opening. However this was not clearly evident from the data obtained. Sample b. shows the presence of moisture in it as there was decrease in impedance. Samples d. e. and g. tend to show normal behavior like the previous samples i.e. increase in impedance with increase in strain.

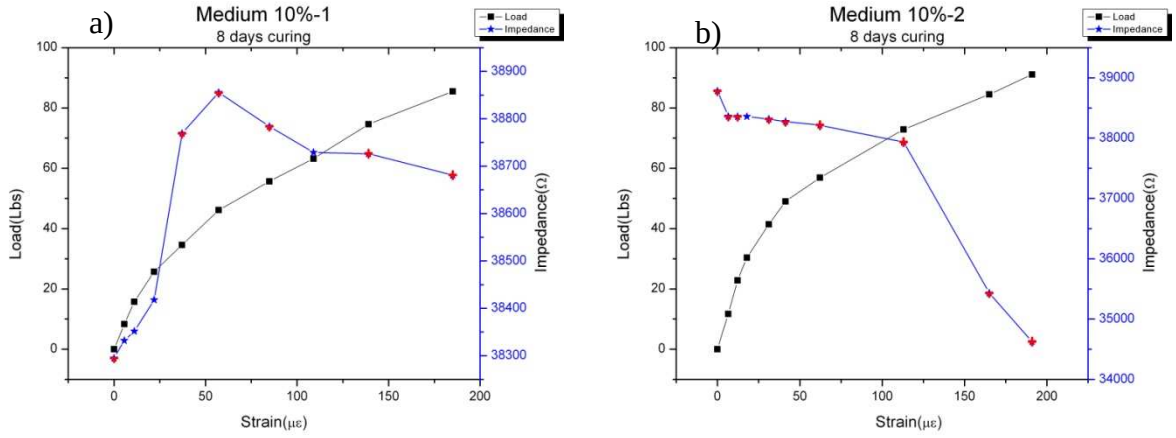

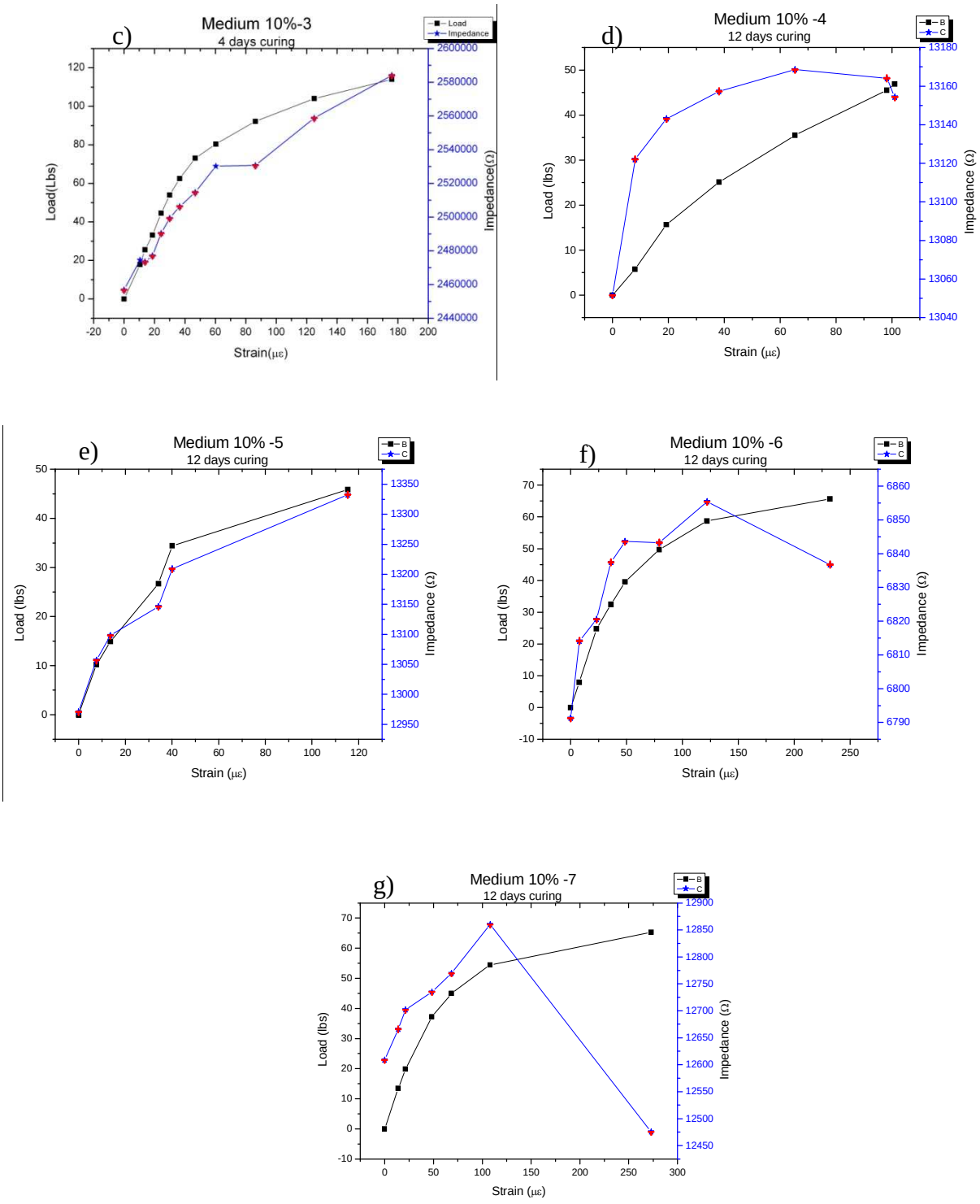

Figure 35: Represents impedance and load as a function of strain of the four concrete samples of 10% strained medium length CNTs a), b) 8 days c) 4 days, d) e) f) g) 12 days curing period

Figure 36 represents the fitted curve of all the six samples of 10% strained medium length CNTs embedded concrete plotted as percentage of maximum impedance being the function of strain. We used a polynomial curve fitting – degree 3 with equation $y = intercept + B_1x^1 + B_2x^2 + B_3x^3$. This curve fitting chosen was the best as it had 73.2% of R-square which represented the measure of fit. From this curve, it can be inferred that impedance increases with crack opening.

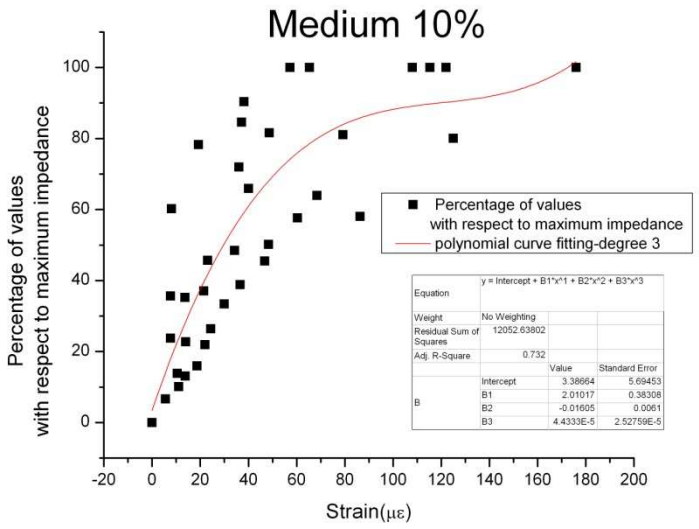

Figure 36: Represents the percentage of values with respect to maximum impedance as a function of strain (curve fitting plot) of the data of four concrete samples containing 10% strained medium length CNTs

6.3.6 Impedance across concrete samples containing 5% wrinkled medium length CNTs

Concrete samples embedded with 5% strained medium length CNTs were cured in the mold for 24hours and later submerged in water. All the five samples made were tested on 14th day, with varied submerged period. Therefore, there was a variation in the absolute impedance values measured across each of the samples but the pattern of impedance for all the samples remained same according to the observed data.

The impedance across every sample was measured at each point of load for three times in an interval of 3 seconds and the mean was plotted. The co-efficient of variance reported in the data

was less than 3% showing a considerable repetition in the data. The results of samples 37 a. b. d. and e. showed that impedance increased with propagation of micro-cracks.

Sample c. showed an increase followed by a decrease in impedance showing a displacement of water pockets in the sample.

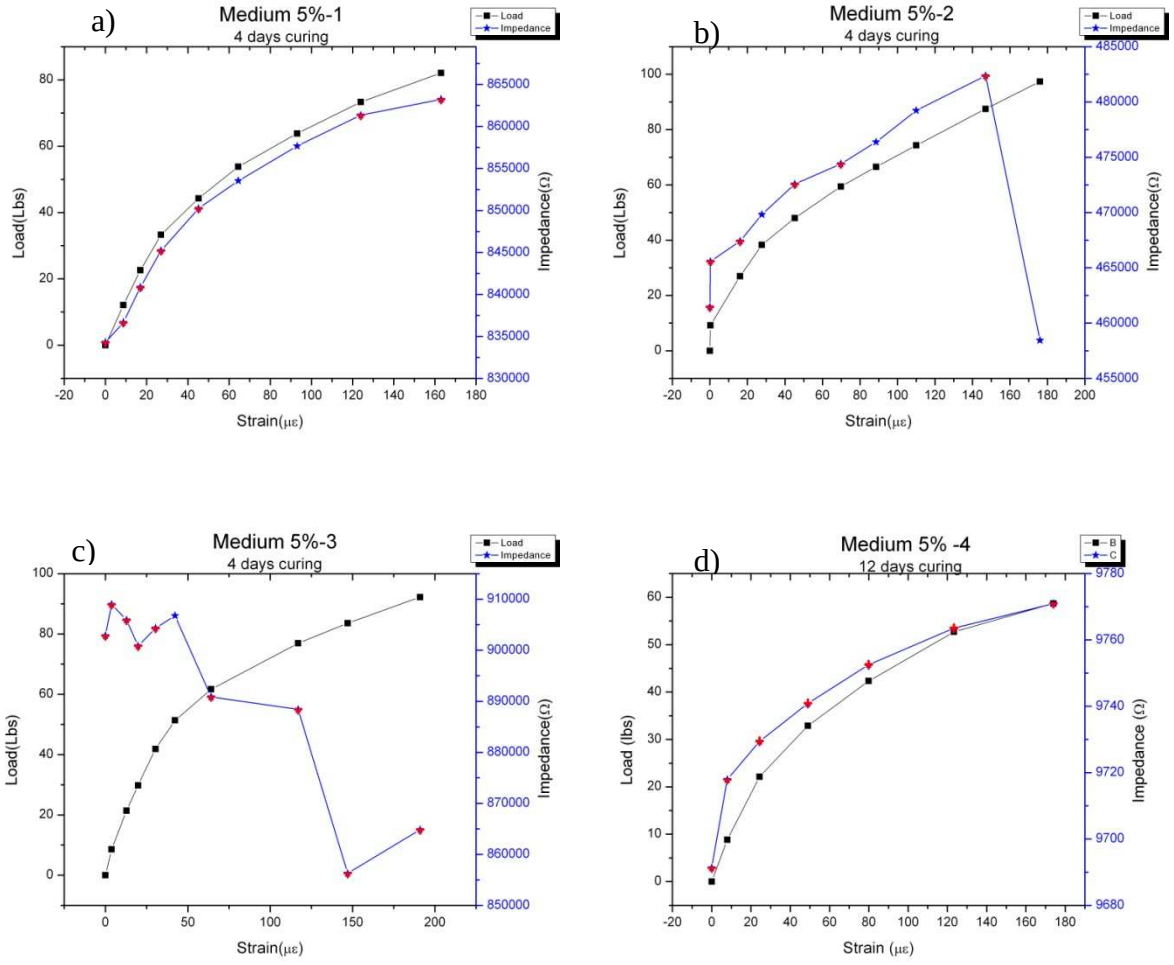

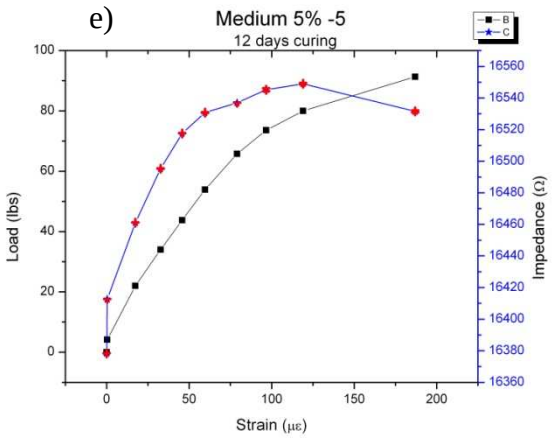

Figure 37: Represents impedance and load as a function of strain of the five concrete samples of 5% strained medium length CNTs a) b) c) 4 days d) e) 12 days curing period

Figure 38 represents the fitted curve of all the five samples of 5% strained medium length CNTs embedded concrete samples plotted as percentage of maximum impedance being the function of strain. We used a polynomial curve fitting – degree 3 with equation $y = intercept + B_1x^1 + B_2x^2 + B_3x^3$. This curve fitting chosen was the best as it had 90.372% of R-square which represented the measure of fit. From this curve, it can be inferred that impedance increases with crack opening.

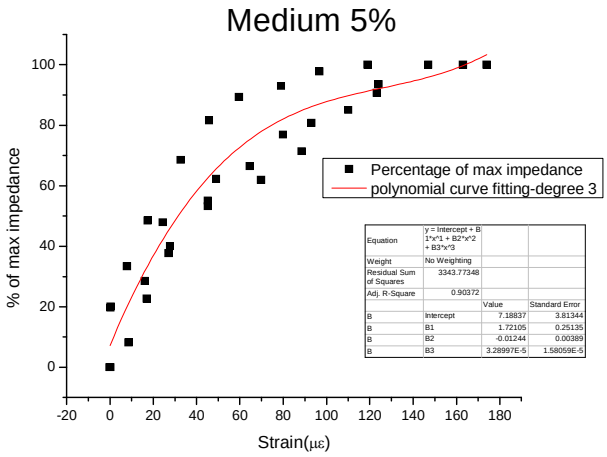

Figure 38: Represents the percentage of values with respect to maximum impedance as a function of strain (curve fitting plot) of the data of four concrete samples containing 5% strained medium length CNTs

6.3.7 Impedance across concrete samples containing 10% wrinkled shorter length CNTs

Concrete samples embedded with 10% strained shorter length CNTs were cured in the mold for 24hours and later submerged in water. All the six samples made were tested on 14th day, with varied submerged period. Therefore, there was a variation in the absolute impedance values measured across each of the samples but the pattern of impedance for all the samples remained same according to the observed data.

The impedance across every sample was measured at each point of load for three times in an interval of 3 seconds and the mean was plotted. The co-efficient of variance reported in the data was less than 5% showing a considerable repetition in the data. The results of samples 39 a. c. d. showed that an increase and a decrease in impedance with propagation of micro-cracks were identified by shorter length carbon nanotubes. Samples b. and e. show the behavior of presence of moisture in them.

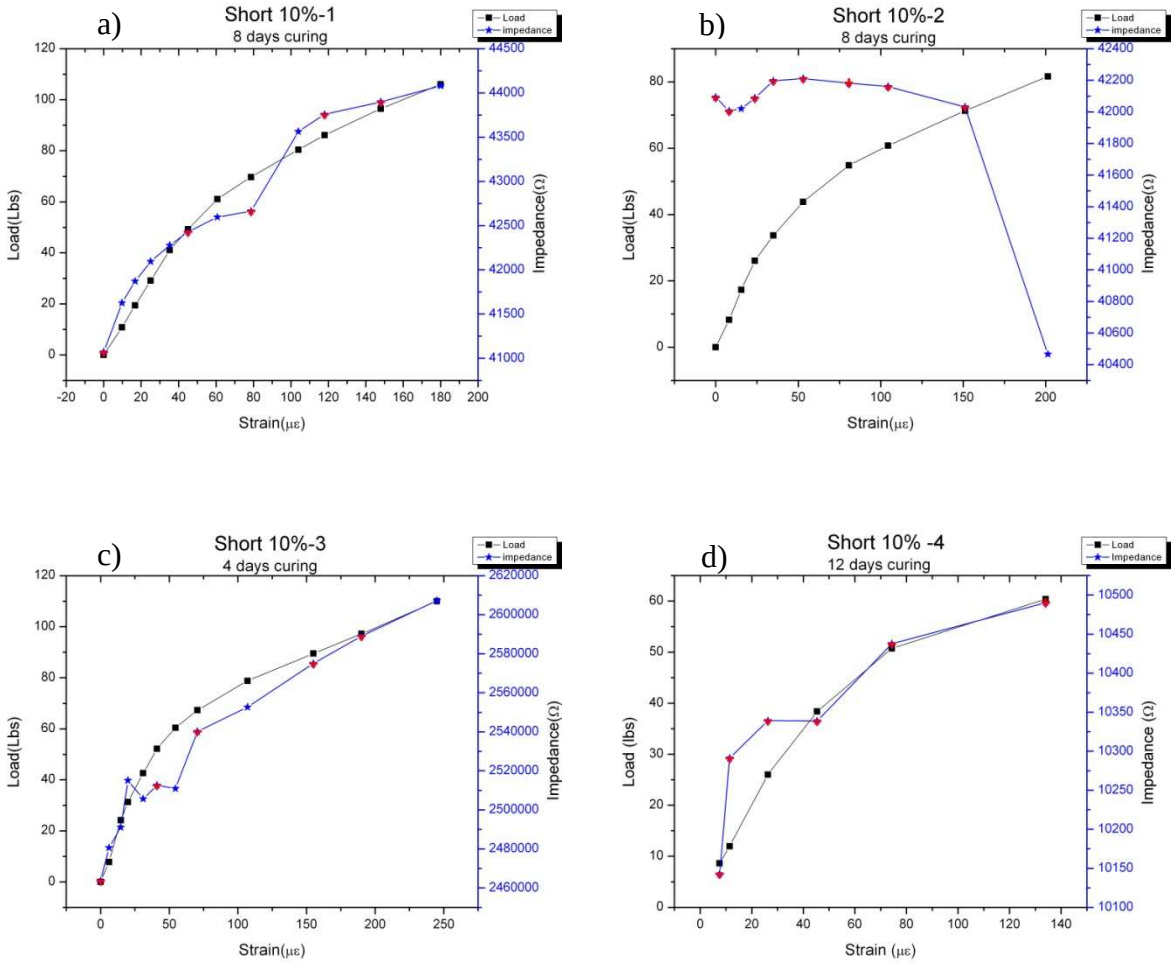

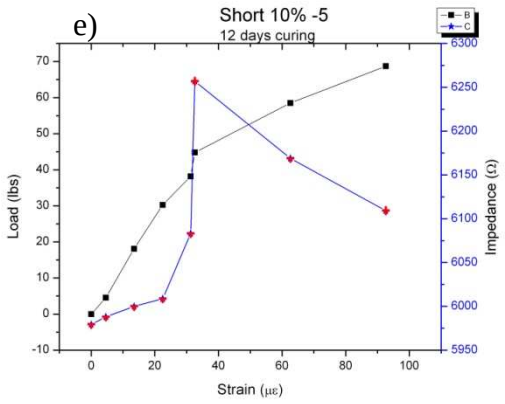

Figure 39: Represents impedance and load as a function of strain of the five concrete samples of 10% strained shorter length CNTs a), 4 days b), c) 8 days, d), e) 12 days curing period

Figure 40 represents the fitted curve of all the five samples of 10% strained shorter length CNTs embedded concrete samples plotted as percentage of maximum impedance being the function of strain. We used an exponential curve with equation $y = y_o + A * \exp(R_o * x)$. This curve fitting chosen was the best as it had 77.885% of R-square which represented the measure of fit. From this curve, it can be inferred that impedance increases with crack opening.

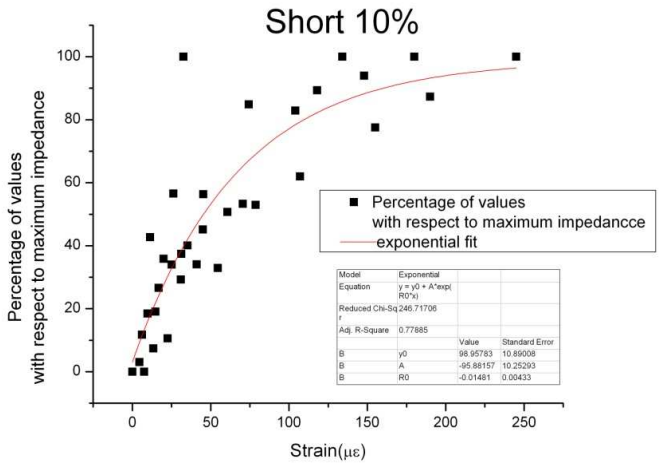

Figure 40: Represents the percentage of values with respect to maximum impedance as a function of strain (curve fitting plot) of the data of four concrete samples containing 10% strained shorter length CNTs

6.3.8 Impedance across concrete samples containing 5% wrinkled shorter length CNTs

Concrete samples embedded with 5% strained shorter length CNTs were cured in the mold for 24hours and later submerged in water. All the six samples made were tested on 14th day, with varied submerged period. Therefore, there was a variation in the absolute impedance values measured across each of the samples but the pattern of impedance for all the samples remained same according to the observed data.

The impedance across every sample was measured at each point of load for three times in an interval of 3 seconds and the mean was plotted. The co-efficient of variance reported in the data was less than 3% showing a considerable repetition in the data. The results of sample a. d. and e. showed that impedance increased with propagation of micro-cracks. Sample c. was sensitive for micro-cracks opening and sample e. had some moisture in it.

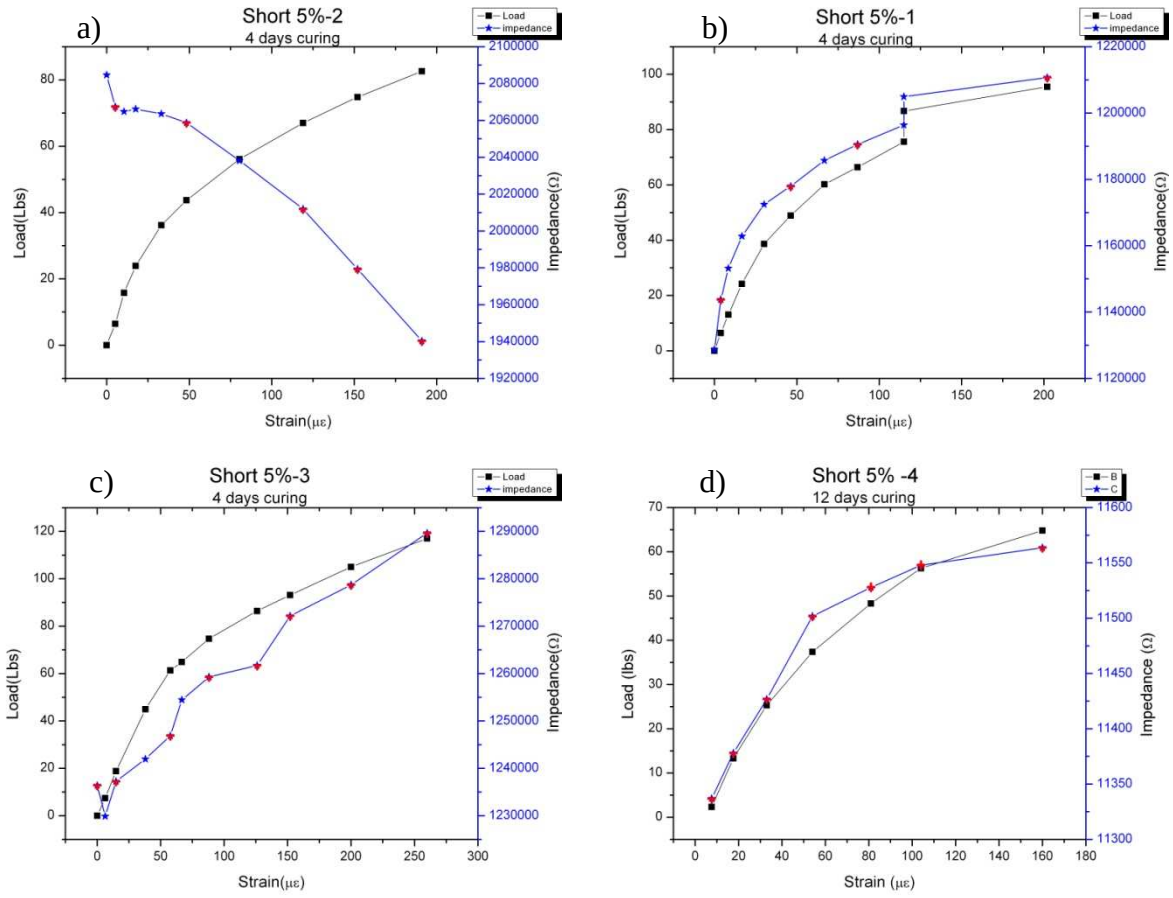

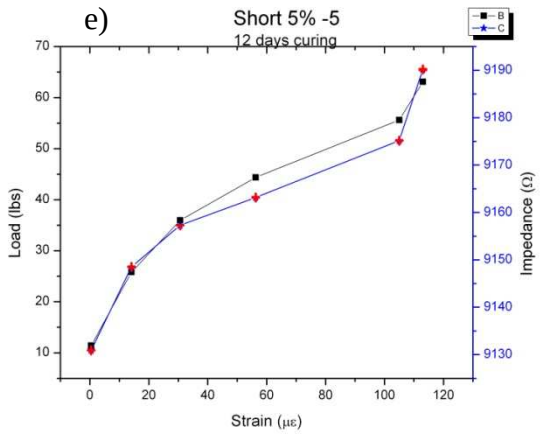

Figure 41: Represents impedance and load as a function of strain of the five concrete samples of 5% strained shorter length CNTs a), b), c) 4 days, d), e) 12 days curing period

Figure 42 represents the fitted curve of all the five samples of 5% strained shorter length CNTs embedded concrete samples plotted as percentage of maximum impedance being the function of strain. We used a polynomial curve fitting – degree 3 with equation $y = intercept + B_1x^1 + B_2x^2 + B_3x^3$. This curve fitting chosen was the best as it had 90.372% of R-square which represented the measure of fit. From this curve, it can be inferred that impedance increases with crack opening.

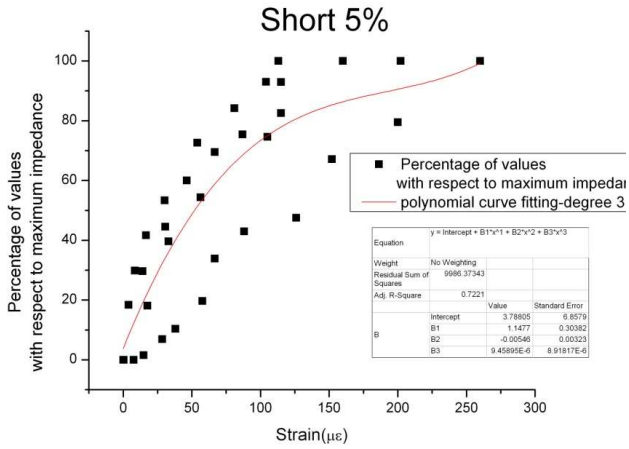

Figure 42: Represents the percentage of values with respect to maximum impedance as a function of strain (curve fitting plot) of the data of four concrete samples containing 5% strained shorter length CNTs

6.3.9 Comparison of percentage of maximum Impedance across concrete samples as a function of strain

Figure 43 shows a comparison of percentage of values with respect to maximum impedance as a function of strain (fitted curves) between mortar sample and mortar sample containing toluene. The graph plotted explained that there was no much variation in the change of impedance between the two sets which clearly showed that adding toluene would not much affect the results obtained.

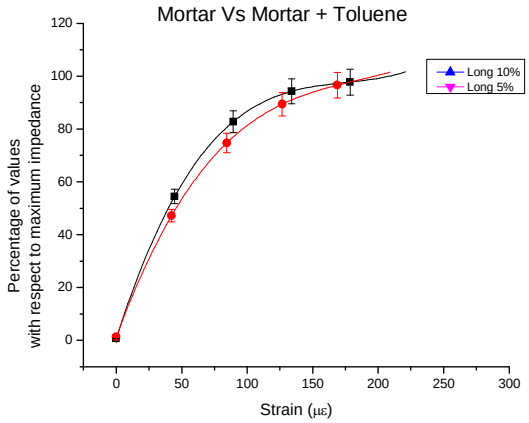

Figure 43: Shows a comparison of percentage of values with respect to impedance as a function of strain between mortar and mortar containing toluene

Figure 44 shows comparison of percentage of values of maximum impedance as a function of strain between 10% wrinkled longer length CNTs and 5% wrinkled longer length CNTs present in concrete sample. The graph plotted for 10% and 5% strained longer length CNTs explained that the change in impedance was observed at the beginning of the non-linear strain proving that 5% long CNTs have better capability than the 10% long CNTs.

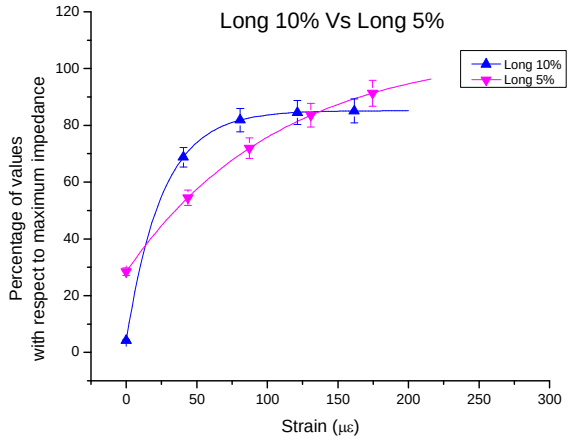

Figure 44: Shows a comparison of percentage of values with respect to impedance as a function of strain between 10% and 5% wrinkled longer length CNTs

Figure 45 gives a comparison of change in percentage of maximum impedance as a function of strain between 10% wrinkled longer length CNTs present in concrete sample and 5% wrinkled medium length CNTs present in concrete sample. The graph plotted explained that the change in impedance curve along with strain proved that 5% strained SWCNTs sensed the crack better than the 10% strained CNTs.

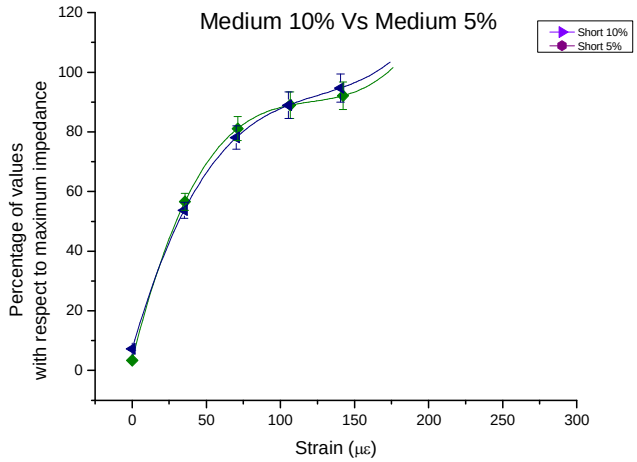

Figure 45: Shows a comparison of percentage of values with respect to impedance as a function of strain between 10% and 5% wrinkled medium length CNTs

Figure 46 shows comparison of percentage of values of maximum impedance as a function of strain between 10% wrinkled medium length CNTs present in concrete sample and 5% wrinkled shorter length CNTs present in concrete sample. The graph plotted explained that the change in impedance curve proved that 5% strained SWCNTs sensed the crack better than the 10% strained CNTs. The non-linear behavior of the curve for 5% has low impedance value than the 10% CNTs.

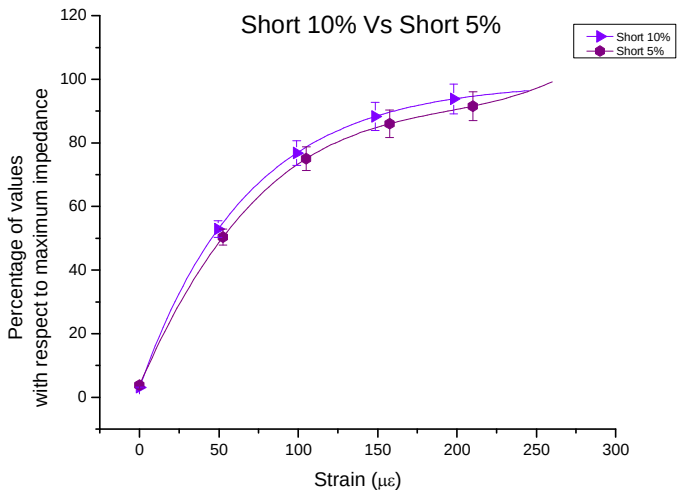

Figure 46: Shows a comparison of percentage of values with respect to impedance as a function of strain between 10% and 5% wrinkled shorter length CNTs

Figure 47 Gives a comparison between long, medium and short 10% strained CNTs working as sensors for defect identification in concrete samples. These samples were subjected to three point bend test and layer 3 was under tension and layer 1 was under compression. As concrete samples are weak in tension, a crack starts to develop from layer 3 and propagates till layer 1. In this process, the conductive layer of CNTs started sensing the cracks and this was reflected in the change in impedance. According to the results obtained, shorter length CNTs showed variation in the change in impedance when compared to medium length CNTs and long CNTs with respect to strain. The crack propagation in the concrete was observed with the non-linearity of the plot along strain Vs impedance.

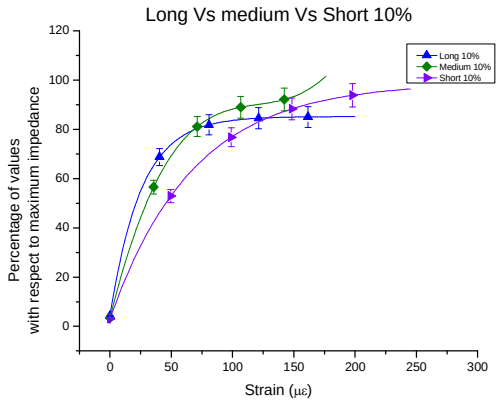

Figure 47: Shows a comparison between long, medium and short 10% strained CNTs

Figure 48 gives a comparison between long, medium and short 5% strained CNTs working as sensors for defect identification in concrete samples. These samples were subjected to three point bend test and layer 3 was under tension and layer 1 was under compression. As concrete samples are weak in tension, a crack starts to develop from layer 3 and propagates till layer 1. In this process, the conductive layer of CNTs started sensing the cracks and this was reflected in the change in impedance. According to the results obtained, shorter length CNTs were good in identifying the cracks when compared to medium and long CNTs during crack propagation. This could be observed from the variation of change in impedance with respect to the non-linear strain.

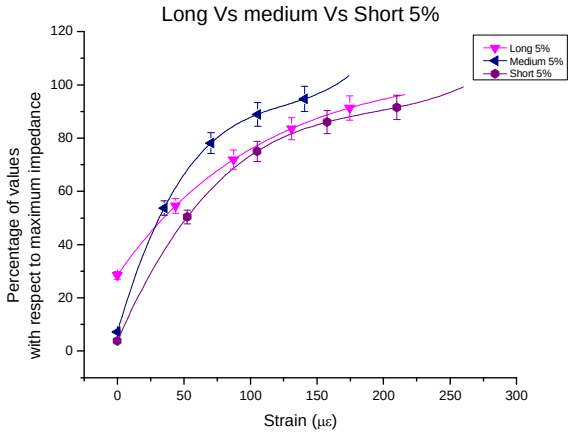

Figure 48: Shows a comparison between long, medium and short 5% strained CNTs

Chapter 7

CONCLUSIONS AND FUTURE WORK

7.1 Conclusion

Identifying the defects in concrete structures were made through non-destructive materials testing (NDMT) which includes electromagnetic radiation, ultrasonic, magnetic particle, liquid penetrant, radiographic, low coherence interferometry, and eddy current testing. But these techniques provided data about cracks in later stages. Various research groups suggested using SWCNT meshes proved to be a good non destructive testing technique which gave precise data about micro-cracks in initial stages.

The experimental results of impedance analysis during curing proved that the amount of moisture content contained in the sample affect the conductivity measurements while testing the sample leads to wrong conclusions. Samples from each set were cured for 4 days, 8 days and 14 days and then were tested on the 14^{th} day. As the curing days decreased, there was an increase in absolute values of impedance but the pattern remained same. This proved that water only affects the absolute impedance values but not the CNTs response for crack detection.

The impedance data for both the 10% wrinkled SWCNTs and the 5% wrinkled CNTs were nearly same, showing that there would be no effect of wrinkling during curing.

The results of samples containing 5% strained longer, medium and shorter SWCNT wrinkled meshes proved that shorter SWCNTs were good in identifying cracks as there was a huge variation in change in percentage of maximum impedance with respect to the initial point of non-linear strain compared to medium and long CNTs samples.

Even in the case of samples containing 10% strained longer, medium and shorter SWCNT wrinkled meshes proved that shorter SWCNTs were good in identifying cracks as there was a huge variation in change in percentage of maximum impedance with respect to the initial point of non-linear strain compared to medium and long CNTs samples.

As the smaller CNTs have more number of junctions, they form better conductive network compared to medium and long CNT network. The better the conductive network, the better identification of cracks explained in figure 49, figure 50 and figure 51.

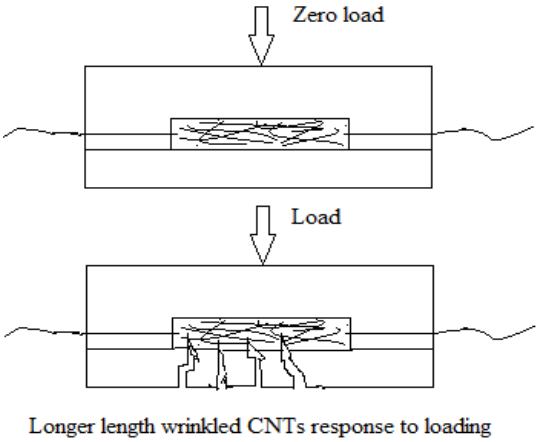

Figure 49: Schematic diagram showing the network of long CNTs in concrete matrix with no load and loading conditions

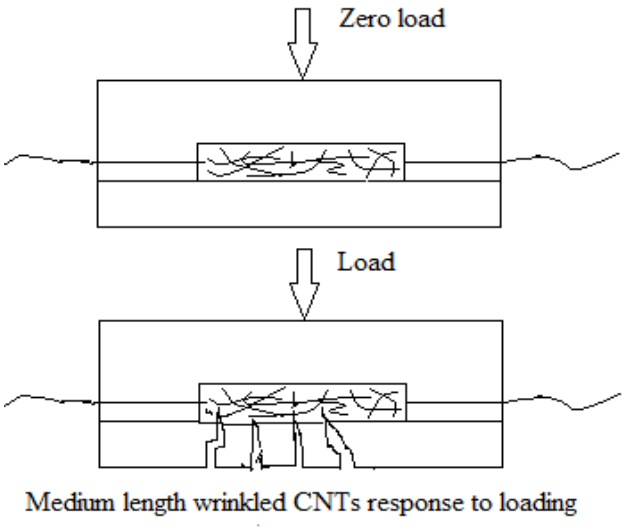

Figure 50: Schematic diagram showing the network of medium CNTs in concrete matrix with no load and loading conditions

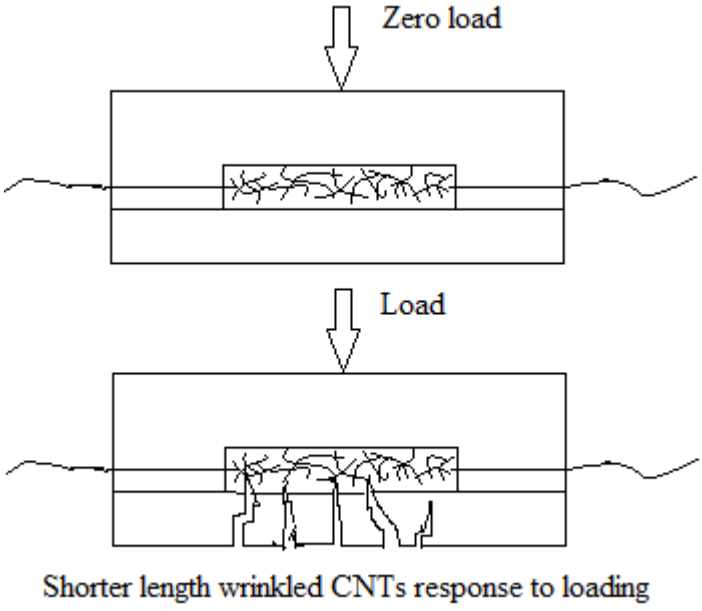

Figure 51: Schematic diagram showing the network of long CNTs in concrete matrix with no load and loading conditions

When compared to the 5% and 10% wrinkled CNTs, 5% showed better results which proved that smaller strain rates of wrinkling have more effect than larger strains.

Adding toluene to mortar samples did not give any variation in the impedance reading while testing the samples as seen from the results of mortar sample and toluene contained mortar sample.

7.2 Future work

From the results obtained from experiments, it was proved that shorter length nanotubes with 5% strain rate of wrinkles were very much effective in detecting the micro-cracks in concrete structures. This will enable the replacement of traditional strain sensors and may be applicable to wide range of applications like pipelines carrying gas and nuclear plants which saves a lot of economy. Samples can be tested on the 28^{th} day and see if there is any variation in the effect of CNTs detecting cracks. Life of a sensor needs to be identified and wrinkling CNTs with varied strain rates has to be focused. Surface crack detection verses onset of cracking in the inner surface can be studied which have its application to wide variety of fields.

REFERENCES

1. **Chamberlain, B.** "Concrete, A Material for the New Stone Age, a MAST Module."*Material Science Technology* (1995)
2. **Hong, Sangdo, and Ronald S. Harichandran.** "Sensors to Monitor CFRP/Concrete Bond in Beams Using Electrochemical Impedance Spectroscopy." *Journal of Composites for Construction* 9, no. 6 (2005): 515-523
3. **ACI Committee 224.** "Causes, Evaluation, and Repair of Cracks in Concrete Structures." In *ACI Journal Proceedings*, vol. 81, no. 3. ACI, 1984
4. **Gunturu, Sai Praneeth,** "Defect Detection in Concrete Structuring Using Homogeneous Length Sorted Single Walled Carbon Nanotube Sensors." Master's Thesis, West Virginia University, 2012
5. **Harris, John M., Ganjigunte RS Iyer, Daneesh O. Simien, Jeffrey A. Fagan, Ji Yeon Huh, Jun Young Chung, Steven D. Hudson et al.** "Structural Stability of Transparent Conducting Films Assembled from Length Purified Single-Wall Carbon Nanotubes." *The Journal of Physical Chemistry C* 115, no. 10 (2011): 3973-3981
6. **Cao, Qing, and John A. Rogers.** "Ultrathin Films of Single-Walled Carbon Nanotubes for Electronics and Sensors: A Review of Fundamental and Applied Aspects." *Advanced Materials* 21, no. 1 (2009): 29-53
7. **Kang, Seong Jun, Coskun Kocabas, Taner Ozel, Moonsub Shim, Ninad Pimparkar, Muhammad A. Alam, Slava V. Rotkin, and John A. Rogers.** "High-Performance Electronics Using Dense, Perfectly Aligned Arrays of Single-Walled Carbon Nanotubes." Nature Nanotechnology 2, no. 4 (2007): 230-236
8. **Makar, J. M., and J. J. Beaudoin.** "Carbon Nanotubes and their Application in the Construction Industry." *Special Publication-Royal Society of Chemistry* 292 (2004): 331-342
9. **McIntosh, Daneesh Olivia,** "Mechanical Properties of Fibers Made from Single Walled Carbon Nanotube Reinforced Thermoplastic Polymer Composites." Master's Thesis, Rice University, 2005
10. **Streitwieser, Andrew, Clayton H. Heathcock, and Edward M. Kosower.** *Introduction to Organic Chemistry*. New York: Macmillan, 1992

11. **Hou, Tsung-Chin, and Jerome P. Lynch.** "Electrical Impedance Tomographic Methods for Sensing Strain Fields and Crack Damage in Cementitious Structures." *Journal of Intelligent Material Systems and Structures* 20, no. 11 (2009): 1363-1379

12. **Raghavan, Ajay, S. Kessler, C. Dunn, Derreck Barber, Sunny Wicks, and Brian L. Wardle.** "Structural Health Monitoring Using Carbon Nanotube (CNT) Enhanced Composites." In *Proceedings of the 7th International Workshop on Structural Health Monitoring, Stanford University*. 2009

13. **Saafi, Mohamed.** "Wireless and Embedded Carbon Nanotube Networks for Damage Detection in Concrete Structures." *Nanotechnology* 20, no. 39 (2009): 395502

14. **Hobbie, E. K., D. O. Simien, J. A. Fagan, J. Y. Huh, J. Y. Chung, S. D. Hudson, J. Obrzut, J. F. Douglas, and C. M. Stafford.** "Wrinkling and Strain Softening in Single-Wall Carbon Nanotube Membranes." *Physical review letters*104, no. 12 (2010)

15. **Ozyildirim, Celik, and Caroline Zegetosky.** "Exploratory Investigation of Nanomaterials to Improve Strength and Permeability of Concrete." *Transportation Research Record: Journal of the Transportation Research Board* 2142, no. 1 (2010): 1-8

16. **Gopalakrishnan, Kasthurirangan, Bjèorn Birgisson, and Peter Taylor, eds.** *Nanotechnology in Civil Infrastructure: A Paradigm Shift*. Springer, 2011

17. **Tjong, S. C.** "Structural and Mechanical Properties of Polymer Nanocomposites." *Materials Science and Engineering: R: Reports* 53, no. 3 (2006): 73-197

18. **Wang, Xueshen, Qunqing Li, Jing Xie, Zhong Jin, Jinyong Wang, Yan Li, Kaili Jiang, and Shoushan Fan.** "Fabrication of Ultralong and Electrically Uniform Single-Walled Carbon Nanotubes on Clean Substrates." *Nano Letters* 9, no. 9 (2009): 3137-3141

19. **Meo, Michele, and Marco Rossi.** "Prediction of Young's Modulus of Single Wall Carbon Nanotubes by Molecular-Mechanics Based Finite Element Modeling."*Composites Science and Technology* 66, no. 11 (2006): 1597-1605

20. **Kim, Hyeon Hwan, and Hyeong Joon Kim.** "Preparation of Carbon Nanotubes by DC Arc Discharge Process Under Reduced Pressure in an Air Atmosphere."*Materials Science and Engineering: B* 133, no. 1 (2006): 241-244

21. **Thess, Andreas, Roland Lee, Pavel Nikolaev, Hongjie Dai, Pierre Petit, Jerome Robert, Chunhui Xu et al.** "Crystalline Ropes of Metallic Carbon Nanotubes."*Science-AAAS-Weekly Paper Edition* 273, no. 5274 (1996): 483-487

22. **Wu, Chi-Hwa.** "Chemical Vapor Deposition of Carbon Nanostructures and Carbon Nanotubes-Reinforced Composites." PhD diss., University of Rochester, 2007

23. **Dresselhaus, M. S., Y. M. Lin, O. Rabin, A. Jorio, A. G. Souza Filho, M. A. Pimenta, R. Saito, Ge Samsonidze, and G. Dresselhaus.** "Nanowires and Nanotubes." *Materials Science and Engineering: C* 23, no. 1 (2003): 129-140

24. **Arnold, K., F. Hennrich, R. Krupke, S. Lebedkin, and M. M. Kappes.** "Length Separation Studies of Single Walled Carbon Nanotube Dispersions." P*hysica Status Solidi (b)* 243, no. 13 (2006): 3073-3076

25. **Asada, Yuki, Toshiki Sugai, Ryo Kitaura, and Hisanori Shinohara.** "Chromatographic Length Separation and Photoluminescence Study on DNA-Wrapped Single-Wall and Double-Wall Carbon Nanotubes." *Journal of Nanomaterials* 2009 (2009): 36

26. **Fagan, Jeffrey A., Matthew L. Becker, Jaehun Chun, Pingting Nie, Barry J. Bauer, Jeffrey R. Simpson, Angela Hight-Walker, and Erik K. Hobbie.** "Centrifugal Length Separation of Carbon Nanotubes." *Langmuir* 24, no. 24 (2008): 13880-13889

27. **Fagan, Jeffrey A., Matthew L. Becker, Jaehun Chun, and Erik K. Hobbie.** "Length Fractionation of Carbon Nanotubes Using Centrifugation." *Advanced Materials* 20, no. 9 (2008): 1609-1613

28. **Dresselhaus, M. S., G. Dresselhaus, R. Saito, and A. Jorio.** "Raman Spectroscopy of Carbon Nanotubes." *Contemporary Concepts of Condensed Matter Science* 3 (2008): 83-108

29. **Portland Cement Association.** "Cement and Concrete Basics." Cement.org. http://www.cement.org/basics/concretebasics_concretebasics.asp

30. Sylgard(R)***;*** Material Safety Data Sheet no. 01015311 [Online]; *Dow Corning Corporation*: Midland, MI, March 15, 2011. http://www3.dowcorning.com/DataFiles/090007b281762143.pdf

31. CG100 Single-walled carbon nanotubes; Data Sheet no. CG 100 [Online]; *South West NanoTechnolgies: Norman, OK, August 26, 2009.* http://swentnano.com/tech/docs/Final_CG_100_Data_Sheet.pdf

32. **Morinobu Endo, Takuaya Hayashi, Yoong Ahm Kim, Mauricio Terrones and Milred S. Dresselhaus**. “Nanotechnology of Carbon and Related Materials”, pp. 2223-

2238 , “*Philosophical Transactions: Mathematical, Physical and Engineering Sciences*”, (2004) 362, No. 1823

33. **Becraft, Eric J., Anton S. Klimenko, and Gregg R. Dieckmann**. "Influence of Alternating L-/D-Amino Acid Chiralities and Disulfide Bond Geometry on the Capacity of Cysteine-Containing Reversible Cyclic Peptides to Disperse Carbon Nanotubes." *Peptide Science 92*, no. 3 (2009): 212-221.
34. **Pfeiffer, R., H. Kuzmany, W. Plank, T. Pichler, H. Kataura, and Y. Achiba**. "Spectroscopic Analysis of Single-wall Carbon Nanotubes and Carbon Nanotube Peapods." *Diamond and related materials 11*, no. 3 (2002): 957-960.
35. **Naaman, Antoine E**. "High Performance Fiber Reinforced Cement Composites: Classification and Applications." *In Proceedings of Cement Based Materials and Civil Infrastructure International Workshop*, Karachi, Pakistan. 2007.
36. **Safarova, K., A. Dvorak, R. Kubinek, M. Vujtek, and A. Rek**. "Usage of AFM, SEM and TEM for the research of carbon nanotubes." *Modern Research and Educational Topics in Microscopy, edited by A. Méndez-Vilas and J. Díaz, Formatex*, Spain 1 (2007): 513-519.
37. **Bellucci, S., G. Gaggiotti, M. Marchetti, F. Micciulla, R. Mucciato, and M. Regi**. "Atomic Force Microscopy Characterization of Carbon Nanotubes." *In Journal of Physics: Conference Series*, vol. 61, no. 1, p. 99. IOP Publishing, 2007.
38. **D F Swnieheart**. "The Beer-Lambert Law." *Journal of Chemical Education 39*, no. 7 (1962): 333.
39. **Shin, Sung Woo, Adeel Riaz Qureshi, Jae-Yong Lee, and Chung Bang Yun**. "Piezoelectric sensor based nondestructive active monitoring of strength gain in concrete." *Smart Materials and Structures* 17, no. 5 (2008): 055002.
40. **Park, Joung-Man, Dae-Sik Kim, Jae-Rock Lee, and Tae-Wook Kim**. "Nondestructive damage sensitivity and reinforcing effect of carbon nanotube/epoxy composites using electro-micromechanical technique."*Materials Science and Engineering: C* 23, no. 6 (2003): 971-975.